



**Quaternized Aryl Ether-Free Polyaromatics for Alkaline  
Membrane Fuel Cells: Synthesis, Properties, and  
Performance – A Topical Review**

Journal:	<i>Journal of Materials Chemistry A</i>
Manuscript ID	TA-REV-06-2018-005428.R1
Article Type:	Review Article
Date Submitted by the Author:	17-Jul-2018
Complete List of Authors:	Park, Eun Joo; Los Alamos National Laboratory Kim, Yu Seung; Los Alamos National Laboratory,

# **Quaternized Aryl Ether-Free Polyaromatics for Alkaline Membrane Fuel Cells: Synthesis, Properties, and Performance – A Topical Review**

Eun Joo Park and Yu Seung Kim\*

MPA-11: Materials Synthesis & Integrated Devices Group, Los Alamos National Laboratory, Los Alamos, New Mexico 87545, United States

## **Abstract**

Quaternized aryl ether-free polyaromatics are an important family of polymer electrolytes for alkaline membrane fuel cells (AMFCs) due to their outstanding alkaline stability. In this review, the state-of-the-art quaternized aryl ether-free polyaromatics are discussed with respect to their synthesis and preparation. The mechanical and electrochemical properties and alkaline stability of the polyaromatics that impact AMFC performance and durability are discussed in comparison with aryl ether-containing polyaromatic and polyolefinic electrolytes. Their performance in membrane electrode assemblies (MEAs) is discussed with emphasis on the area specific resistance and phenyl group adsorption on hydrogen oxidation catalysts. AMFC performance of MEAs employing state-of-the-art aryl ether-free polyaromatics is compared with those employing polyolefin and aryl ether-containing polyaromatics. Finally, limitations and outlook of quaternized aryl ether-free polyaromatics are briefly summarized.

\* yskim@lanl.gov

## 1. Introduction

Alkaline membrane fuel cells (AMFCs) are an attractive alternative to acidic proton exchange membrane fuel cells (PEMFCs) because inexpensive non-platinum group metal (PGM) catalysts can be used for the alkaline oxygen reduction reaction (ORR).<sup>1</sup> One of the major hurdles for developing high-performing AMFCs has been the stability of hydroxide-conducting polymer electrolytes under high pH fuel cell operating conditions.<sup>2</sup> Polymer electrolytes are utilized as anion exchange membranes (AEMs) and catalyst ionomeric binders in AMFCs; AMFCs generate electricity from fuels via electrochemical reactions where an AEM conducts hydroxides from the cathode to the anode while separating fuels and oxidant in the system and where ionomeric binders provide hydroxide conducting pathways for the higher catalyst activity as well as mechanical tenacity in the electrodes. Over the last decade, significant efforts have been made to improve the alkaline stability of hydroxide-conducting polymer electrolytes for highly durable AMFCs.

Fig. 1 portrays the gradual increase in the number of research articles on the topic related to the development of hydroxide-conducting polymer electrolytes used in AMFCs since 2007. The most studied class of alkaline polymer electrolytes is quaternized polyaromatics, which take more than 60% of the total number of research articles published in the last 5 years. Polyaromatics, including both aryl ether-free and aryl ether-containing, were followed by olefinic-type polymer electrolytes include polyethylene, polypropylene and polystyrene-based polymers synthesized from functionalized alkene monomers, and “others” include perfluorinated, composite or alkali-metal-doped polymer electrolytes. The outstanding number of publications dealing with quaternized polyaromatics is primarily because it is relatively easy to tailor their structures compared to other types of polymer electrolytes, indicating the importance of their position as alkaline polymer electrolytes.

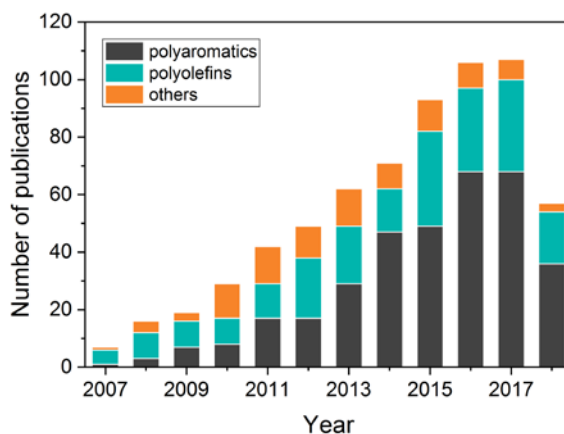


**Fig. 1** Number of research articles on polymer electrolyte membranes for AMFCs over the 10 years (as of May 8, 2018). The related articles were found with keywords “alkaline membranes” and “fuel cells” from Web of Science™, Thomson Reuters, and then categorized based on their polymer backbone structure.

In this review, we provide a comprehensive description of the synthesis, properties, and performance of quarternized polyaromatics with aryl ether-free backbones, known for the most stable electrolytes under high pH conditions. For this, we first provide a brief background and significance of the polyaromatics for AMFC applications. Next, the most up-to-date list of reactions to synthesize the aryl ether-free polyaromatics and their quaternization methods to form the corresponding AEM are discussed with their advantages and disadvantages. In the following section, the mechanical and electrochemical properties of the polyaromatics are discussed with respect to their chemical structure. Moreover, the chemical stability of the polyaromatics under high pH conditions is compared with aryl ether-containing polyaromatics and polyolefinic electrolytes. Finally, the performance of quaternized aryl ether-free polyaromatics in MEAs is discussed, emphasizing the area specific resistance (ASR) and phenyl group adsorption. The AMFC performance employing state-of-the-art aryl ether-free polyaromatics is compared with those employing other polymer electrolytes. The limitations and future research challenges of quaternized aryl ether-free polyaromatics for advanced AMFCs are briefly shared for future direction.

## 2. Background of Quaternized Aryl Ether-Free Polyaromatics

Quaternized polyaromatics as alkaline polymer electrolytes were first suggested in 1985 by Zschocke and Quellmalz who demonstrated an excellent alkaline stability of non-quaternized poly(aryl ether sulfone)s.<sup>3</sup> The initial synthetic efforts to prepare quaternized polyaromatics mostly relied on the base-catalyzed nucleophilic aromatic substitution reaction using activated dihalide and dihydroxyl monomers followed by post-polymerization modification to introduce cationic groups. From this synthetic route, each repeating unit of polymers contains aryl ether (C–O) linkages along the main chain of the polymer. Although such heteroatom linkages may allow rotational freedom along the polymer backbones, which help to improve the solubility of resulting polymers, Fujimoto et al. and Arges et al. proposed that such polymers have a high possibility of undergoing backbone cleavage at C–O bonds via hydroxide attack (Fig. 2a).<sup>4, 5</sup> The following studies from other research groups further elucidated that the polymer backbone cleavage at C–O bonds takes place much faster when an electron-withdrawing cation is located in close proximity to the backbone.<sup>6-8</sup> The impact becomes more severe when the adjacent phenyl ring contains electron-withdrawing substituents, for example, perfluoro group or sulfone linkage, which causes the electron deficiency of the ring, thus increases vulnerability towards the backbone cleavage (Fig. 2b). Moreover, Miyanishi and Yamaguchi suggested that decomposition of cation groups is not derived from the instability of the ionic group itself, but rather triggered by the cleavage of nearby ether bonds.<sup>9</sup> Even when the backbone is not functionalized with ionic groups, the presence of C–O bonds in the main chain may cause hydroxyl radical initiated degradation of the membrane in fuel cell operating conditions.<sup>8, 10</sup> Thus, aryl ether-containing polyaromatics are not suitable for the long-term operation of AMFCs, and polymer main chain degradation needs to be resolved to improve the overall durability of AMFCs.

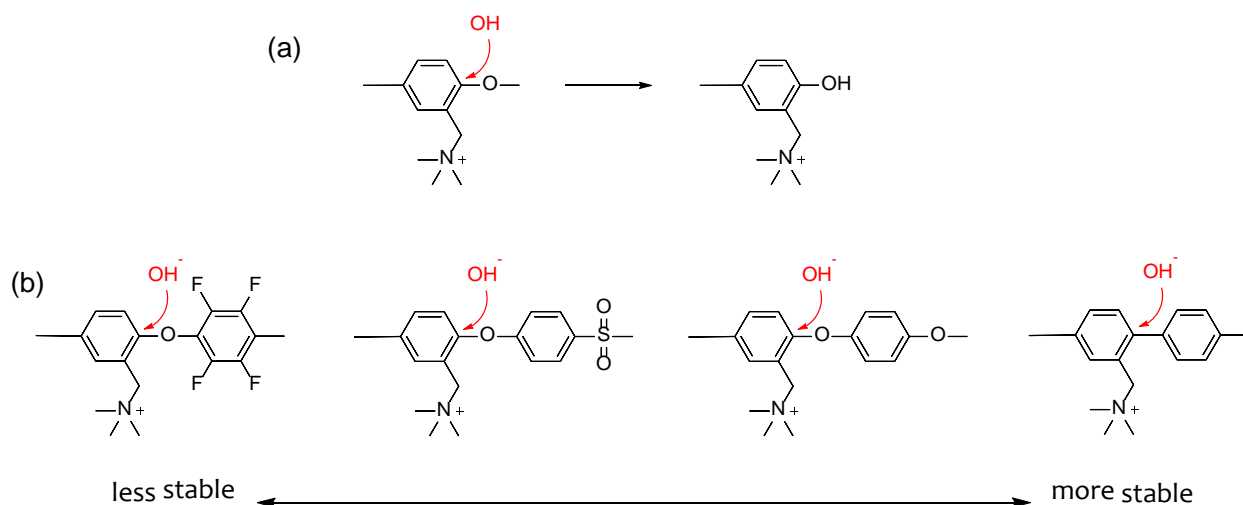


**Fig. 2** (a) Aryl ether cleavage of quaternized aryl ether-containing polymer backbone and (b) the comparison of the polymer backbone stability of various polyaromatics.<sup>4, 6, 7</sup>

One of the most promising approaches to resolve the chemical stability of polymeric materials used in AMFCs is to prepare aryl ether-free polyaromatics. This approach allows the polymer electrolytes to possess desirable characteristics of polyaromatic backbone such as high glass transition temperature, high impact strength and toughness and good thermal, chemical and mechanical stability and low water uptake compared to polyolefinic electrolytes.<sup>11-13</sup>

With the alkaline stable polyaromatic backbone structure, the alkaline stability of functionalized cations on the polyaromatics is crucial to ensure the long-term stability. Tetraalkylammonium ionic species are the most widely used cations for polymer electrolytes in AMFCs, and the way they are tethered to the polymer backbone and the alkyl side chain structure largely affect their stability in alkaline condition. In general, representative small cation molecules are synthesized to compare their thermochemical stability in basic condition and investigate potential degradation mechanism in order to elucidate the relationship between chemical structure and alkaline stability.<sup>14-16</sup> Pivovar et al. demonstrated earlier that benzyltrimethylammonium (BTMA) cations have much better alkaline stability than phenyltrimethylammonium cations.<sup>17, 18</sup>

The BTMA group on polyaromatics is the most common cationic functional group due to their widely practiced post-polymerization functionalization method despite their vulnerability towards the nucleophilic hydroxide attack. Adding a different length of alkyl extender chains pendant to the ammonium to induce phase separation was reported to increase cation stability.<sup>19</sup> Lately, it is generally accepted that the cation group placed on pendant electron-donating alkyl spacer chains along the backbone improves microphase separation, ion conductivity and overall alkaline stability of polymer electrolytes.<sup>20-22</sup> A number of studies demonstrated that the optimum conductivity and alkaline stability were achieved by having 5 or 6 carbon atoms in the flexible alkyl spacer unit between cations and the backbone.<sup>23, 24</sup> Using more hydrophilic spacers, for instance, ethylene oxide instead of alkyl spacers, may improve the thermal stability and ion conductivity of polymer electrolytes.<sup>25</sup> Stabilized imidazolium and rotationally restricted piperidinium cations are also suggested as alternative cation moieties with enhanced alkaline stability.<sup>15, 26</sup> Various cation structures have been successfully incorporated into aryl ether-free polyaromatics due to the synthetic viability of facile chemical modification of aromatic rings.

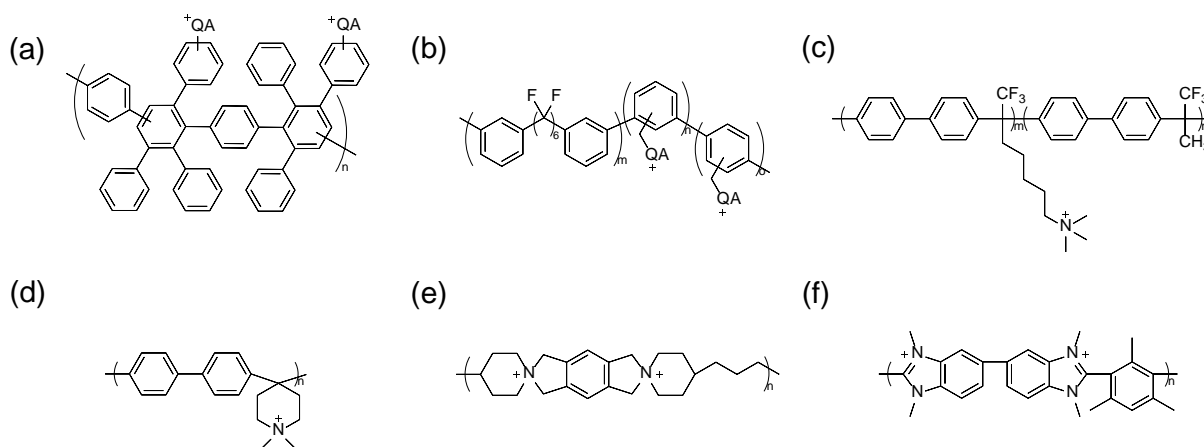


**Fig. 3** Representative molecular structures of different quaternized polymers with aryl ether-free backbones: (a) Diels-Alder poly(phenylene), (b) poly(perfluoroalkyl phenylene), (c) poly(biphenyl alkylene), (d) poly(biphenylene piperidinium), (e) spiro-ionene and (f) poly(mesityl-dimethyl benzimidazolium).

### 3. Synthesis of Aryl Ether-Free Polyaromatics and Quaternization

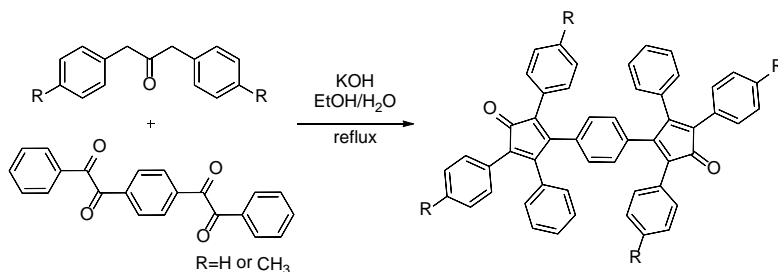
Fig. 3 illustrates some examples of quaternized aryl ether-free polymers that we will address in this section. Since there are not many aryl ether-free polyaromatic backbones commercially available for post-functionalization, different synthetic methods to form such backbone have been developed. The different synthetic methods, as well as the type of cationic groups and ion exchange capacity (IEC), offer a structural diversity that determines the properties of the polymers, which we will discuss in the next section.

#### 3.1 Diels-Alder Polymerization

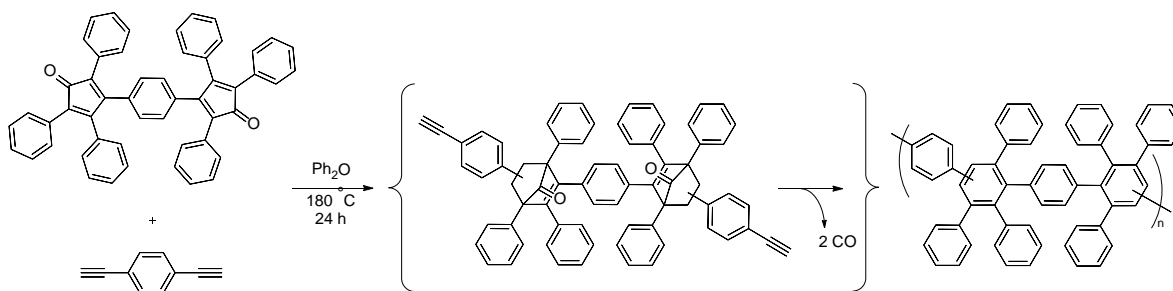
Polymers with a high molecular weight backbone composed of wholly aromatic C–C bonds have found many applications requiring high thermochemical and oxidative stability. The Diels-Alder reaction, a concerted [4+2] cycloaddition between a conjugated diene and a dienophile into a cyclohexene, became one of the most useful reactions in organic synthesis for a wide variety of applications since the time it was first discovered.<sup>27, 28</sup> Due to the possibility of forming entirely aromatic backbone polymers,<sup>29</sup> poly(phenylene)s made by Diels-Alder polymerization (DAPP) may be suitable for polymer electrolyte membranes. DAPP-based ion exchange membrane was first utilized as proton exchange membranes upon post-sulfonation, which showed good proton conductivity and thermochemical stability.<sup>30</sup> It is one of the earliest examples of ion exchange membranes made of fully aromatic polymers absent of heteroatoms. The polymer was then further employed as AEMs upon quaternary ammonium (QA) group-functionalization on the DAPP backbone.<sup>20, 31</sup>

The key monomers to synthesize the backbone of DAPP, bis(cyclopentadienone) and its derivatives, are not commercially available, so they need to be synthesized via multiple-step reactions (Scheme 1).<sup>32, 33</sup> Based on the substituents on 4,4'-dimethylbis(benzyl ketone), the

backbone may have methyl groups for further functionalization.<sup>31</sup> The other monomer for the polymerization, 1,4-diethynylbenzene, is commercially available. Upon the thermally induced reaction followed by the removal of carbon monoxide, DAPP with six pendant phenyl groups per repeating unit in random *para*- and *meta*-configuration could be produced (Scheme 2).<sup>29</sup> The random configuration of phenyl groups improves solubility of the polymers in common organic solvents leading easy preparation, characterization, and processing and prevents electron conduction. The good solubility of DAPP is a great merit because poly(phenylene)s with linear *para*-configuration usually exhibit poor solubility due to the structural stiffness.<sup>34</sup>



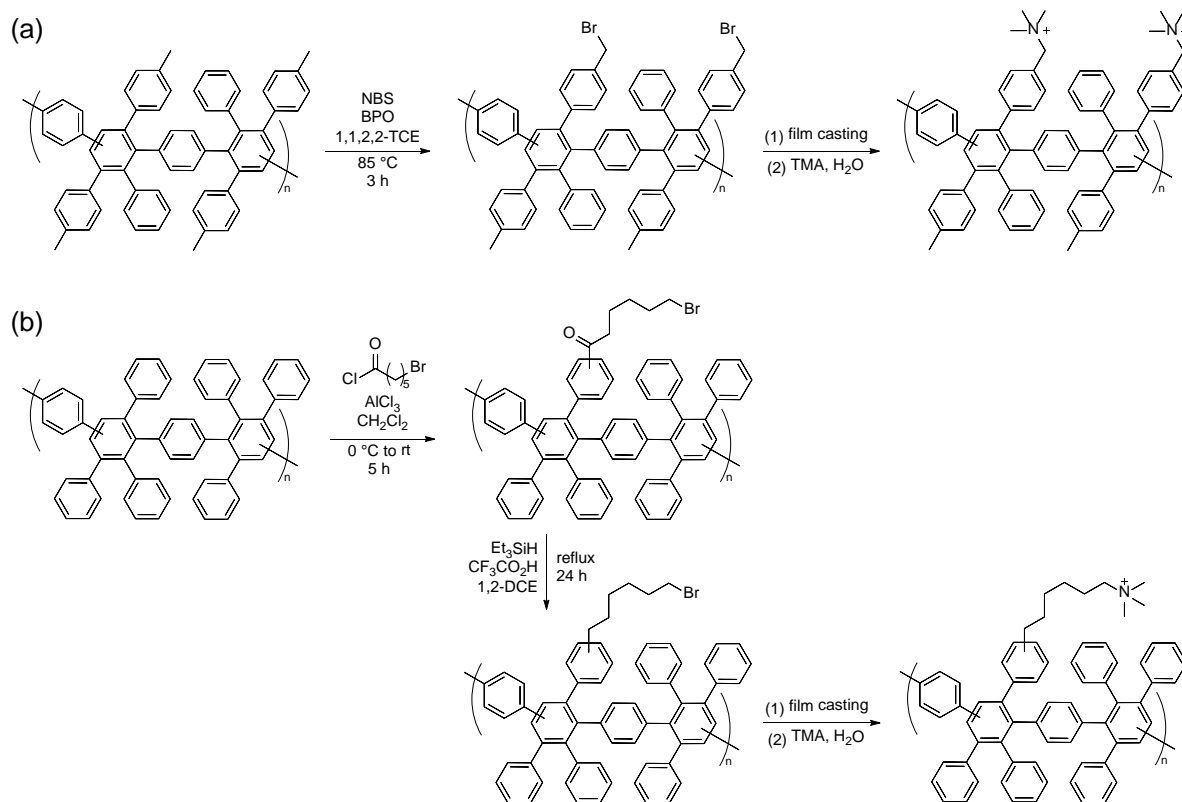
**Scheme 1** Synthesis of the monomer, bis(cyclopentadienone), for the Diels-Alder reaction.



**Scheme 2** The general polymer backbone synthesis of DAPP.

The quaternization processes of DAPP to form various structures of cations are depicted in Scheme 3. BTMA-functionalized DAPP (ATMPP) was prepared on the methylated DAPP by a radical bromination reaction followed by  $S_N2$ -type amination using TMA (Scheme 3a).<sup>31</sup> The degree of bromomethyl group was controlled by the amount of the brominating reagent. The

bromomethylated DAPP was cast as a film using chloroform and treated with aqueous TMA solution to afford the quaternized membrane. Only 55-75% of the bromomethyl group was converted into the QA group due to less effective heterogeneous quaternization.



**Scheme 3** Quaternization of poly(phenylene)s: (a) synthesis of ATMPP via bromination/amination and (b) synthesis of TMAC6PP via Friedel-Crafts acylation/reduction/amination. NBS=*N*-bromosuccinimide, BPO=benzoyl peroxide, 1,1,2,2-TCE=1,1,2,2-tetrachloroethane, TMA=trimethylamine and 1,2-DCE=1,2-dichloroethane.

Taking the cation stability into account, different cations besides BTMA were functionalized on the DAPP backbone.<sup>20</sup> Benzyl pentamethylguanidinium and benzyl *N*-methylimidazolium were functionalized using the similar scheme to prepare ATMPP using pentamethylguanidine and *N*-methylimidazole, respectively, instead of TMA (Scheme 3a). The quaternization reaction occurred in solution-state, yielding the nearly quantitative conversion.

The DAPP-based AEM with a trimethylammonium cation attached by an electron-donating hexamethylene spacer, TMAC6PP, was synthesized by Friedel-Crafts acylation, followed by reduction of the resulting ketone linker and quaternization using TMA, as described in Scheme 3b.<sup>20</sup> The downside of this quaternization method is the requirement of stoichiometric amounts of Lewis acid,  $\text{AlCl}_3$ , as the metal catalyst, which is not environmentally friendly. The cation structures achieved by different quaternization routes were subjected for measurement of ion conductivity and alkaline stability, which will be further discussed in Section 4.

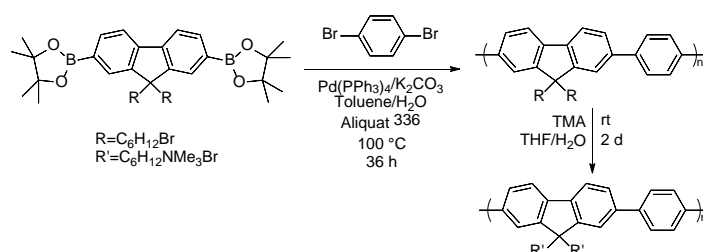
Among the reactions forming phenylene-based polymers, Diels-Alder polymerization offers several advantages including (i) metal-free condition to avoid potential contamination of metals of the resulting materials, (ii) irreversibility for high molecular weight growth and (iii) good solubility and thus good processability of the resulting polymer for sequential quaternization. Some drawbacks may include that DAPPs require higher molecular weight compared to other polyaromatics to obtain good mechanical properties due to its rigid and stiff nature of the polymer backbone entirely composed of phenyl rings.<sup>4</sup> Also, the bulky backbone structure may lead to high free volume between the polymer chains, which may increase the reactant gas permeability compared to linear polymers.<sup>35</sup> Furthermore, the synthetic limitation of incorporating cation precursor moieties to its monomer for easy quaternization also requires multiple-step post-polymerization functionalization for the AEM application of these materials.

### 3.2 Metal-catalyzed Coupling Reactions

Transition-metal-catalyzed cross-coupling reactions are another class of reactions that have been utilized in polymer chemistry to build a polymer backbone composed of aromatic C–C bonds. The polyaromatics made by the synthetic method commonly feature their  $\pi$ -conjugated backbone structure as well as the good chemical and thermal stabilities and used widely for optical and

electronic applications.<sup>36</sup> The aryl-aryl bond formation via cross-coupling reactions usually occurs between aryl halides and related electrophiles with the aid of organometallic catalysts, and the most ubiquitously used transition-metal catalysts are palladium- or nickel-based complexes.<sup>37</sup> The prerequisites for a successful preparation of high molecular weight polymers using these reactions are solubility of the monomers and the resulting polymer in the reaction medium, and the inertness of the monomers with the metal catalysts.<sup>38</sup>

The Suzuki coupling reaction employing aromatic boronic acids/boronate esters with aromatic bromide compounds in the presence of a palladium-complex is widely used for fluorene-based copolymers, which are extensively studied in the light-emitting diodes related fields.<sup>39, 40</sup> Fluorene-based AEMs without heteroatoms in the backbone structure was first introduced by Lee et al. with hexyl spacer-tethered QA groups as the cation group (Scheme 4).<sup>41</sup> Two bromoalkyl groups were incorporated at the 9-position of the boronate ester-containing fluorene monomer and used for facile quaternization. Three different dibromo compounds were utilized to form different alternating copolymer structures as shown in Fig. 4. The alkyl bromide-containing precursors were synthesized by the palladium-catalyzed Suzuki coupling reaction. Trimethylhexyl quaternary ammonium (TMHA) group was obtained via a Menshutkin reaction of TMA with the precursor polymers in solution-state.



**Scheme 4** Synthesis of quaternized poly(fluorene-benzene) (PFB) via Suzuki coupling.

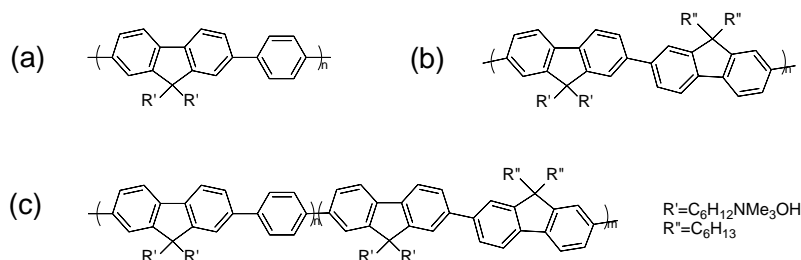
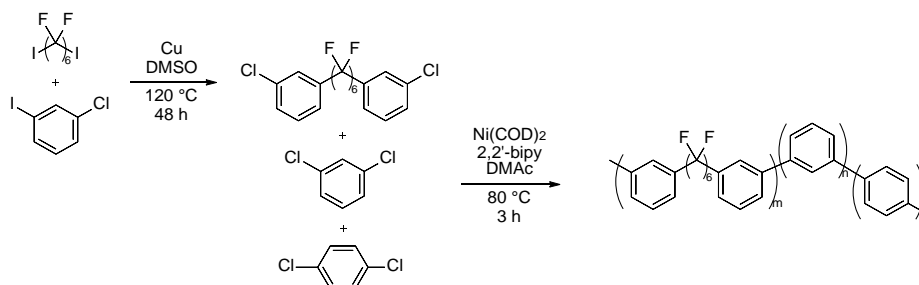


**Fig. 4** Polymer structure of poly(fluorene)-based AEMs: (a) PFB, (b) poly(fluorene-fluorene) (PFF) and (c) poly(fluorene-benzene-fluorene-fluorene) (PFBFF).

Polymerization of aryl halides using nickel-catalyzed coupling is known for a versatile and efficient method to synthesize a variety of high-performance phenylene polymers.<sup>42, 43</sup> Miyatake et al. reported aromatic membranes composed of perfluoroalkylene and quaternized oligophenylene groups via the nickel-catalyzed coupling reaction (Scheme 5 and Fig. 5ab).<sup>44, 45</sup> The hydrophobic perfluoroalkylene monomer was synthesized via Ullmann coupling reaction using Cu as a catalyst (Scheme 5). The resulting monomer contains aryl chloro-groups at both ends, which were used for nickel-catalyzed polymerization with two different dichlorobenzene monomers, *m*-dichlorobenzene, and *p*-dichlorobenzene. The <sup>1</sup>H NMR spectra showed that the reactivity of *m*-phenylene is higher than *p*-phenylene. The perfluoroalkylene copolymers (PAF) showed a high polydispersity index (PDI) of 5.7 possible due to the different reactivity of the aryl halide monomers of different sizes.



**Scheme 5** Synthesis of the polymer backbone of PAF via the nickel-catalyzed coupling reaction.

The QA ionic group was obtained via chloromethylation followed by quaternization. Here in the PAF system, only *n* and *o* blocks are subjective towards chloromethylation due to the electron deficiency of aryl groups adjacent to the electron-withdrawing perfluoroalkyl group.<sup>44</sup> Since chloromethylation lacks a precise control on the placement of the functionality, the chloromethyl groups were placed randomly in *m*- and *o*-phenylene groups (the hydrophilic group), and subsequently quaternized using TMA, dimethylbutylamine (DMBA), dimethylhexylamine, or 1,2-dimethylimidazole.<sup>44, 45</sup>

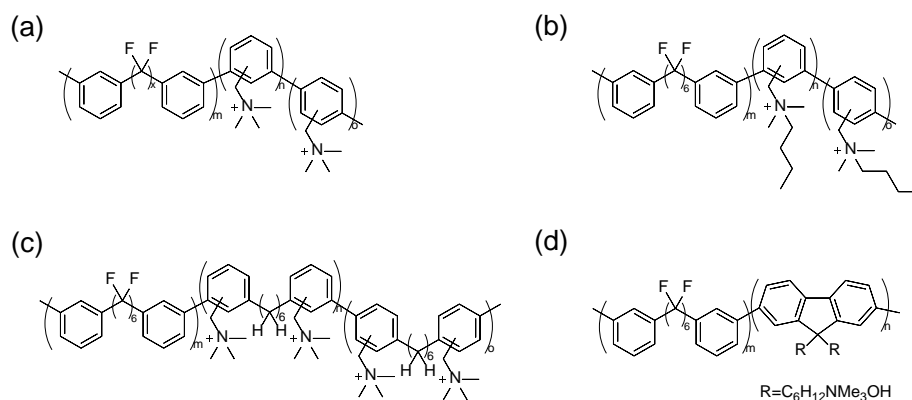


**Fig. 5** The molecular structure of QPAF series polymers: (a) QPAF-TMA, (b) QPAF-DMBA, (c) QPAF-3 and (d) QPAF-4.

Miyatake and co-workers investigated different backbone structure using alkylene-containing monomers (Fig. 5c)<sup>46</sup> and fluorene-containing monomer (Fig. 5d).<sup>47</sup> The polymerization was done using the same synthetic procedure using nickel-catalyzed coupling described in Scheme 5. The fluorene-containing PAFs showed the high polydispersity index (10.2-17.4), which indicate that Suzuki coupling would be more efficient to form fluorene-based polyaromatics with a narrower polydispersity.

Beside the PAF copolymers, nickel-catalyzed polymerization was utilized to form different polymer electrolyte structures and used as AEMs. The monomers used for the polymerization

largely influence the alkaline stability of the resulting polymers. Holdcroft et al. synthesized a dichloro *m*-terphenyl monomer with benzimidazole to form poly(phenylene) bearing 1-methylbenzimidazolium (PPMB, Fig. 6a).<sup>48</sup> The *m*-terphenyl backbone protects benzimidazolium to have high alkaline stability, which will further discussed in Section 3.5. On the other hand, although the backbone of the imidazolium-containing poly(phenylene) synthesized by the coupling reaction does not contain alkaline labile C–O bonds on the backbone (Fig. 6b),<sup>49</sup> the final polymer structure has alkene and benzophenone in the repeating unit, which may undergo side reactions in high-temperature alkaline media.<sup>20</sup> These two examples may show the importance of choosing monomers for polymerization to have alkaline stable polyaromatic materials.

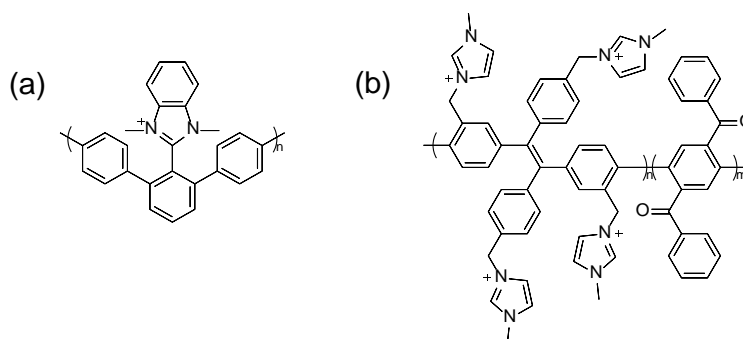


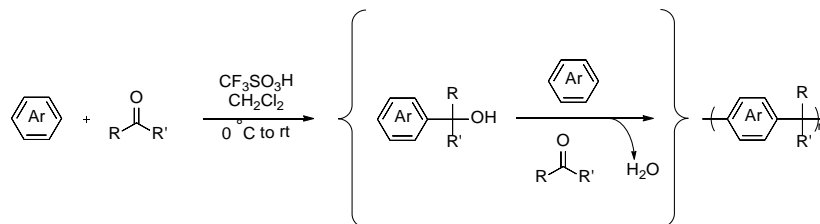
**Fig. 6** The molecular structure of poly(phenylene) with (a) 1-methylbenzimidazolium and (b) imidazolium synthesized via nickel-catalyzed polymerization.

Palladium- and nickel-catalyzed cross-coupling reactions have been demonstrated as highly effective and practical methods for the construction of aryl ether-free backbone polyaromatics. Suzuki coupling reactions may allow facile incorporation of fluorene-moieties in the polymer structure. The downside of the utilization of Suzuki coupling reactions is the requirement of expensive palladium metal catalysts and boron-containing monomers, which would economically limit the approach thus scaling-up synthesis of the materials. While nickel-catalyzed polymerization is cost-effective due to less expensive nickel catalysts and aryl chloride monomers,

it should be noted that a large quantity of nickel catalyst is required for polymerization (2.5 equivalent molar amount of aryl chloride monomers<sup>44</sup>). In addition, the polydispersity of the polymers made by nickel-catalyzed polymerization may vary depending on the reactivity of the aryl chloride monomer used.

### 3.3 Acid-catalyzed Friedel-Crafts Polyhydroxyalkylation

Strong Brønsted or Lewis acid are known to enhance the reactivity of electrophiles via superelectrophilic activation.<sup>50</sup> Superelectrophilic activation can play a significant role in Friedel-Crafts condensation of ketones and aldehydes with arenes to construct C–C bonds. Zolotukhin et al. first demonstrated the superacid-catalyzed polyhydroxyalkylation reaction for the preparation of linear polyaromatics.<sup>51–53</sup> The general synthetic route involves trifluoromethanesulfonic acid (also known as triflic acid, TFSA), one of the Brønsted superacids, to catalyze the growth of polymer chains by superelectrophilic activation of fluorinated carbonyl-containing ketone compounds with aromatic hydrocarbons in dichloromethane at room temperature (Scheme 6). The polymerization is highly regioselective for 4- and 4'-position of the terminal aryl rings of the aromatic monomer, which can lead to high molecular weight of the linear polymer.<sup>52</sup> The reaction time varies depending on the monomer reactivity;<sup>54</sup> once the molecular weight of the polymer increases, it starts to form a reactive gel-like precipitate causing phase separation from the initially homogeneous solution.<sup>51</sup> After completion of polymerization, the reaction mixture is poured into methanol to quench the remaining acid and precipitate the polymer. Upon purification, the product is obtained as fibrous polymers. Depending on the choice of carbonyl-containing electrophilic monomers and phenyl monomers, this polymerization method can construct a wide variety of polyaromatics with different structures for diverse applications.

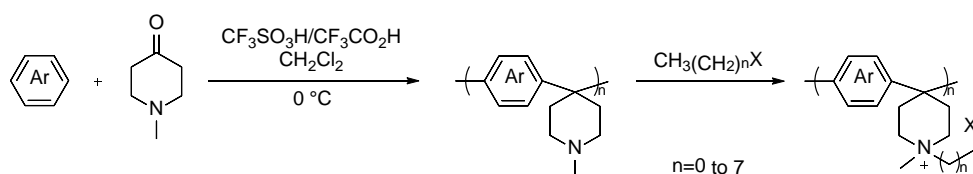


**Scheme 6** General scheme of acid-catalyzed Friedel-Crafts polyhydroxyalkylation.

Lee et al. reported a series of long and flexible side-chain cations-tethered poly(phenyl alkylene)s synthesized via acid-catalyzed polymerization.<sup>55, 56</sup> Polymerization of one phenyl monomer (biphenyl (BPN1-*m*, Fig. 3c, where *m* indicates the mol% of the ionic repeating unit),<sup>55</sup> *p*-terphenyl (*p*-TPN1) or *m*-terphenyl (*m*-TPN1)<sup>56</sup>) and trifluoromethylalkyl ketone monomers (7-bromo-1,1,1-trifluoroheptan-2-one and 1,1,1-trifluoroacetone) in different ratios generated polyaromatic AEMs with variable IECs. In order to incorporate a cationic functional group to the backbone of the polyaromatic, 7-bromo-1,1,1-trifluoroheptan-2-one was prepared according to a procedure in the literature<sup>57</sup> to provide a bromopentyl side chain used for quaternization. The acidic reaction condition for the polymer synthesis allowed having a potential leaving group, alkyl bromide, which can be easily replaced with a tertiary amine to afford a QA group; this would not be feasible in base-catalyzed polycondensation because of the nucleophilic nature of the polymerization condition. The IEC of the resulting membranes was controlled using different ratios of the trifluoromethylalkyl ketones. The alkyl bromide was subsequently converted into trimethylpentyl ammonium (TMPA) bromide via a Menshutkin reaction. In spite of the backbone structure constructed with rigid aromatic rings, the resulting ionic polymers exhibited good solubility in polar organic solvents probably due to the presence of a tetrahedral  $sp^3$ -carbon between biphenyl rings of the polymer main chain. However, *p*-terphenyl-based polymer showed

the lower solubility compared to *m*-terphenyl- and biphenyl-based polymers, most likely because of the more rigid *para*-terphenyl moieties.

More recently, the reaction was employed by Jannasch et al. to synthesize poly(arylene piperidinium) AEMs using commercially available *N*-methyl-4-piperidone as the ketone monomer (Fig. 3d, Scheme 7).<sup>58</sup> The resulting polymer contains aromatic and piperidine rings, and the following alkylation affords piperidinium-functionalized AEMs. Prior to the study, the authors confirmed the thermochemical stability of the piperidinium model compound, 4,4-diarylpiperidinium, which led them to prepare the corresponding AEMs using biphenyl (PBPIP) and *p*-terphenyl (PTPIP) as the phenyl monomer. The use of an electron-withdrawing trifluoromethyl group-absent ketone monomer caused the polymerization process to yield lower molecular weight polymers, indicated by intrinsic viscosity measurement, compared to other polyaromatics. The authors mentioned that the solubility of PTPIP is slightly poorer than PBPIP because of the stiffer molecular structure of the former, which is the same as the previous finding.<sup>56</sup> Due to the reasonable water uptake after the membrane formation, PTPIP were further studied after quaternization using different alkyl bromides, butyl-, hexyl-, and octyl bromide, to form the AEMs with different length of alkyl extender chain (PTPIPQ<sub>n</sub>, *n*=the number of carbon atoms of the extender chain). Zhuang et al. also synthesized the *p*-terphenyl incorporated poly(arylene piperidinium) (QAPPT) via the same procedure followed by methylation to yield a membrane.<sup>59</sup>



**Scheme 7** Synthesis of the backbone of poly(arylene piperidine) followed by alkylation to form PBPIPQ<sub>n</sub>, PTPIPQ<sub>n</sub>, and QAPPT.

The molecular weight of poly(arylene piperidinium) could grow higher by using 2,2,2-trifluoroacetophenone as a co-monomer along with the piperidine ketone monomer (Fig. 7); the  $M_w$  of the poly(terphenylene piperidinium) was up to 70 kg/mol.<sup>60</sup> The higher reactivity of the electron-deficient ketone monomer is beneficial for the polymerization to form AEMs with higher mechanical strength.

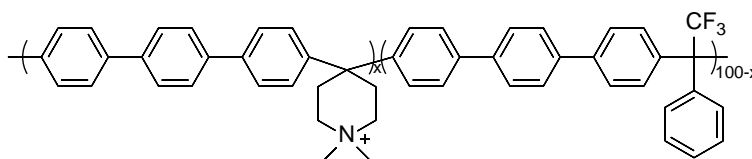


**Fig. 7** The molecular structure of poly(terphenylene piperidinium).

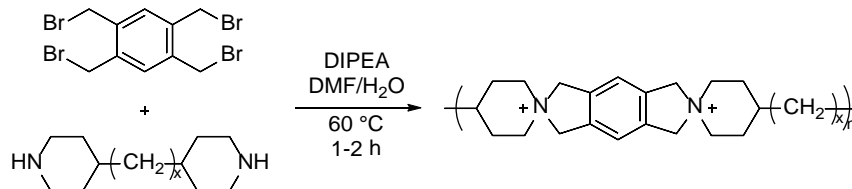
The key advantages of using acid-catalyzed Friedel-Crafts polyhydroxyalkylation include (i) simple one-step synthesis, (ii) metal-free condition and (iii) formation of polyaromatics with the  $sp^3$ -carbon containing flexible backbone structure. Thanks to the good solubility of the ionic polymers made by the process, the polymers may find their use as ionomer binding materials for fuel cell electrodes. In addition, since QA-precursors (alkyl bromide<sup>55, 56</sup> and tertiary amine<sup>58</sup>) are acid-tolerant, they can be incorporated in the polymer structure at the polymerization stage, and then quaternization can be achieved by a simple Menshutkin reaction with tertiary amine and alkylation using alkyl bromide, respectively. Hence the degree and the location of the QA group is much more precisely controlled, and post-polymerization modification including chloromethylation,<sup>61</sup> radical bromination,<sup>62</sup> lithiation,<sup>63</sup> and C–H borylation<sup>64</sup> is not required. One thing to note is that in order to form high molecular weight polymers for the robust mechanical stability of the membrane, a discrete choice of ketone monomers with electron-withdrawing moieties would be necessary to allow successful superelectrophilic activation and growth of long polymer chains to promote intermolecular chain entanglement for membrane mechanical strength.

### 3.4 Cyclo-polycondensation

Ionene polymers are polymers with ammonium groups in the backbone, commonly synthesized via a repetitive alkylation reaction of dihalides with diamines or polycondensation of bifunctional haloamines.<sup>65</sup> They have been used as materials for many applications including conductive polymers, polyelectrolyte complexes in aqueous solutions, biomedical application, and so on.<sup>66</sup> The synthesis of polymeric aromatic ionenes with spirane structure using tetrabromomethylbenzene and secondary diamine was reported by Müllen et al.,<sup>67</sup> demonstrating the possibility of the formation of dication compounds and polymeric ionenes using the chemistry. Besides the cation centering between 5- and 6-membered rings, the ionene polymer synthesized by the cyclo-polycondensation reaction does not contain other heteroatom linkages or electron-withdrawing groups in the backbone.

This useful chemistry was adopted to prepare high molecular weight, film-forming AEMs by Jannasch et al. (Scheme 8). Two *N*-spirocyclic QA ionenes (spiro-ionene **1** and **2**,  $x=0$  and  $3$ , respectively) containing cations in the polymer backbone were prepared and characterized.<sup>68</sup> The tetrabromide monomer, 1,2,4,5-tetrakis(bromomethyl)benzene, was synthesized by radical bromination of durene using an excess of NBS and azobisisobutyronitrile. The two dipiperidine monomers, 4,4'-bipiperidine and 4,4'-trimethylenedipiperidine, were commercially available. The spiro-polycondensation reaction is a two-step process, deprotonation and attack of a nitrogen in piperidine on one of the bromoalkyl group and then intramolecular quaternization leading a 5-membered ring formation and a QA cation. The chemical structure of the backbone incorporating cations with spirane structure might be particularly beneficial for the use as AEMs due to the reported high alkaline stability of 6-azonia-spiro[5.5]undecane at elevated temperature.<sup>15</sup> The

central QA cation fused in 6-membered rings exhibited high resistance against both nucleophilic substitution and elimination likely because of the constrained geometry of the rings.



**Scheme 8** Synthesis of *N*-spirocyclic QA ionene **1** and **2**,  $x=0$  and  $3$ . DIPEA=*N,N*-diisopropylethylamine.

Since the chemical structure of the polymer contains two cations per repeating unit without having any pendant group, the density of ionic sites is higher than other ionic polymers, leading the polymer water-soluble,<sup>68</sup> which would not be practical for the direct use in the aqueous membrane-based fuel cell system. The authors demonstrated the preparation of blend membranes with commercially available poly(benzimidazole). The  $-\text{NH}-$  groups of poly(benzimidazole) are partially deprotonated by the spiro-ionene, which may help to increase the interaction between two polymeric materials for better mechanical strength and prevention of the spiro-ionene leaching.

The notable features of the preparation of AEMs using cyclo-polycondensation would be that the reaction proceeds under mild conditions (60 °C) for the short period of time (1-2 hours) in the presence of moisture (the co-solvent for the reaction is water). The main difference of the polymeric ionenes from the previously introduced polymers made by the different synthetic routes is that the former has ionic groups directly integral in the polymer main chain while the latter contains ionic groups as the pendant group on the side chain. The nature of cyclo-polycondensation directly leads to the formation of cationic groups and the polymer backbone, which is simple, however, the resulting polymers own high IECs that reduce their mechanical stability and limit the practical applicability without physical modification.

### 3.5 Others

A small structural variation can help to improve the stability and physical properties of a known material; poly(benzimidazole) can be one example. poly(benzimidazole) is a commercially available synthetic fibrous material, featuring high molecular weight, high melting point, and material toughness.<sup>69</sup> Phosphoric acid-doped poly(benzimidazole) have been extensively utilized for high-temperature PEMFCs.<sup>70</sup> However, its quaternized analogue, poly(dimethyl benzimidazolium), was not suitable for the use in AMFCs due to the chemical susceptibility on the imidazolium C2 position towards nucleophilic attack by hydroxide ions, causing ring opening and degradation of the polymer backbone (Fig. 8a).<sup>71, 72</sup> The alkaline stability of the C2-substitution of imidazolium salts was investigated by Yan et al., and their study suggested that the steric hindrance effect of the substituents protects the imidazolium cation, in addition to the hyperconjugative effect increasing electron density around the cations.<sup>73</sup>

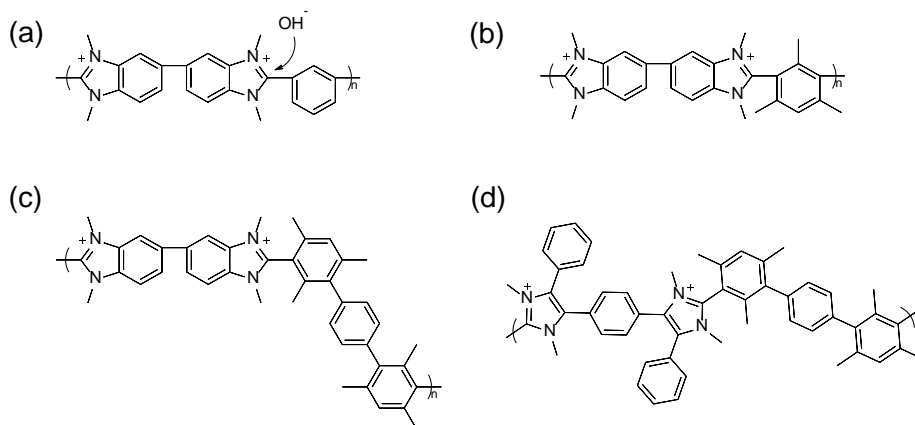
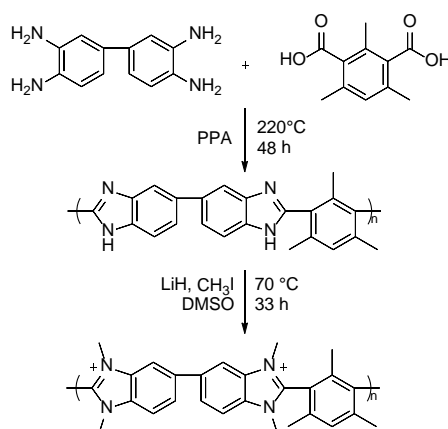


**Fig. 8** The molecular structure of (a) poly(dimethyl benzimidazolium) and the potential nucleophilic attack of hydroxide ions on the imidazolium C2 position, (b) poly[2,2'-(*m*-mesitylene)-5,5'-bis(*N,N'*-dimethylbenzimidazolium)]), Mes-PDMBI, (c) HMT-PDMBI and (d) HMT-PMPI.

Holdcroft et al. have reported the synthesis of the stabilized derivative of poly(dimethyl benzimidazolium) by providing steric protection of the benzimidazolium C2 position using an

adjacent bulky mesityl group.<sup>74</sup> A mesitylene-containing diacid monomer, 2,4,6-trimethylisophthalic acid, was synthesized via a four-step process and polymerized with 3,3'-diaminobenzidine in polyphosphoric acid (PPA) to form mesityl-protected poly(benzimidazole) (Fig. 8b and Scheme 9).<sup>74</sup> The PPA and hydrolyzed compounds need to be removed by washing thoroughly with water after the reaction. The polymer was further deprotonated and then followed by the methylation to afford the cationic-containing polymer. Since the polymerization process is known to yield high molecular weight poly(benzimidazole) in the given condition (high polymerization temperature in PPA), they are considered to be sufficiently high in molecular weight to be used for AMFC applications.



**Scheme 9** The polymer backbone synthesis of Mes-PDMBI.

Similar to the spiro-ionenes discussed in Section 3.4, Mes-PDMBI, where the ionic portion is part of the polymer main chain with a relatively small repeating unit size, showed a high IEC value and the water-solubility,<sup>74</sup> which limits its use as an AEM or a catalyst ionomeric binder. The polymer had to be insolubilized by blending with different ratio of poly(benzimidazole) in DMSO, which lowers the IEC of the resulting materials. Such limitation was improved by using 2,2'',4,4'',6,6''-hexamethyl-*p*-terphenylene (HMT) instead of the mesitylene of Mes-PDMBI to

form HMT-PDMBI, and the increased hydrophobicity of the polymer backbone led the polymer to be water-insoluble, which no longer requires the blending process (Fig. 8c).<sup>75</sup>

Holdcroft et al. further extended the system by developing poly(arylene-imidazolium), HMT-PMPI (Fig. 8d).<sup>76</sup> From the study using different sterically protected imidazolium small molecules, the structure with *ortho*-methyl phenyl on the C2 position of imidazolium showed the highest alkaline stability; therefore, the polymer analogue was synthesized using microwave-assisted polycondensation of dialdehyde and bisbenzil. The new synthetic routes for aryl ether-free polymer backbone inspired by the poly(benzimidazole) structure expanded the variety of the promising chemically stable AEM materials.

Besides polymer blending blend approach, pore-filling membrane approach has been attempted to improve the properties of ionic polymers. The idea of pore-filling of porous substrates using cross-linkable monomers was practiced to effectively generate thermally and mechanically stable polymer electrolytes for fuel cells.<sup>77-79</sup> Yamaguchi and co-workers demonstrated the synthesis of the cross-linked aromatic backbone polymer with highly packed anion-exchange sites using the pore-filling method.<sup>80</sup> An aryl monomer with three tertiary amine groups was synthesized and converted to three BTMA groups upon *in situ* cross-linking with dichloroxylylene in the pores of a polyethylene porous substrate. Such physical modification may enhance various material properties of polymer electrolytes, including lower water uptake, less fuel cross-over, high mechanical strength and high durability.

### 3.6 Summary of the Synthetic Methods for Aryl Ether-free Polyaromatics

Before wrapping up the section, we provide a summarized table to compare different synthetic methods for aryl ether-free polyaromatics to help the readers' understanding of the differences of the processes (Table 1).

**Table 1.** Summary of different synthetic methods for aryl ether-free polyaromatics.

Synthetic method (Section)	Examples	QA location	Cationic group	IEC (meq./g)	$M_w$ (kg/mol)	PDI	Notes	Ref.
<b>Diels-Alder polymerization (3.1)</b>	Diels-Alder poly(phenylene)	Side chain	BTMA Guanidinium Imidazolium TMHA	0.93-2.40	121-172	2	<ul style="list-style-type: none"> <li>• Metal-free polymerization</li> <li>• Some monomers are not commercially available</li> <li>• High free volume, may have fuel crossover issues</li> <li>• QA precursor incorporation is limited</li> <li>• Low IEC polymer does not have good solubility</li> </ul>	20, 30, 31
<b>Pd-catalyzed coupling reaction (3.2)</b>	Poly(fluorene)	Side chain	TMHA	2.45-3.59	30-78	2.6	<ul style="list-style-type: none"> <li>• Good solubility in polar aprotic solvents and methanol</li> <li>• Ideal for incorporation of fluorene-moieties</li> <li>• Requires expensive Pd catalysts and boron-containing monomers</li> </ul>	41
<b>Ni-catalyzed coupling reaction (3.2)</b>	Poly(perfluoro alkylene phenylene)	Side chain	BTMA, DMBA Alkyl ammonium Imidazolium	0.49-1.74	28-90	5.7	<ul style="list-style-type: none"> <li>• Good solubility in polar aprotic solvents, methanol and ethanol</li> <li>• Less expensive nickel catalysts</li> </ul>	44-46
	Poly(fluorene phenylene)	Side chain	TMHA	0.74-2.14	73-276	14	<ul style="list-style-type: none"> <li>• A large quantity of the catalysts is required</li> </ul>	47
	Poly(phenylene)	Side chain	benzimidazolium	2.56	129	NA	<ul style="list-style-type: none"> <li>• PDI varies</li> </ul>	48
<b>Acid-catalyzed Friedel-Crafts polyhydroxyalkylation (3.3)</b>	Poly(phenyl alkylene)	Side chain	TMPA	1.46-2.70	106-139	1.8	<ul style="list-style-type: none"> <li>• Metal-free polymerization</li> <li>• Facile incorporation of QA precursors</li> </ul>	55, 56
	Poly(arylene piperidinium)	Side chain	piperidinium	1.98-2.65	Low-70	NA	<ul style="list-style-type: none"> <li>• Excellent solubility in low boiling point alcohol solvents (OH<sup>-</sup> form)</li> <li>• Choice of monomers is important for molecular weight growth</li> </ul>	58-60
<b>Cyclo-polycondensation (3.4)</b>	Spiro-ionone	Main chain	Spiro-cyclic QA	4.0-4.6	67-80 <sup>a</sup>	NA	<ul style="list-style-type: none"> <li>• Mild reaction condition for the short period of time</li> <li>• High IEC leads solubility in water</li> <li>• The physical modification process is required</li> </ul>	68
<b>Others (3.5)</b>	Poly(dimethylbenzimidazolium)	Main chain	benzimidazolium	4.5	NA	NA	<ul style="list-style-type: none"> <li>• High IEC leads solubility in water</li> <li>• The physical modification process is required</li> </ul>	74, 75
	Poly(arylene imidazolium)	Main chain	imidazolium	2.61	67	1.4	<ul style="list-style-type: none"> <li>• Soluble in water in high temperature</li> </ul>	76
	Cross-linked polymer	Main chain	BTMA	1.98	NA	NA	<ul style="list-style-type: none"> <li>• <i>In situ</i> crosslinking using cross-linkable monomers in the porous substrate</li> </ul>	80

<sup>a</sup> obtained from <sup>1</sup>H NMR spectra.

## 4. Properties Related to AMFC Performance

Table 2 shows the summary of the material properties of quaternized aryl ether-free polyaromatics discussed in the previous section. For comparison purposes, the material properties of other families of alkaline polymer electrolytes, i.e. quaternized aryl ether-containing polyaromatics and polyolefins, are also included.

**Table 2.** Properties of different backbone AEMs.

Polymer backbone	Sample name	IEC (meq./g)	Molecular weight ( $M_w$ , kg/mol)	Tensile strength (MPa) <sup>a</sup>	Elongation to break (%) <sup>a</sup>	Water uptake (wt.%) <sup>b</sup>	Anion conductivity (mS/cm) <sup>b</sup>	Backbone synthesis	ref
<b>Aryl ether-free polyaromatics</b>									
DAPP	ATMPP	1.90	77/196	28/32 (50, 50)	19/47 (50, 50)	159 (- <sup>c</sup> , OH <sup>-</sup> )	18 (rt, Cl <sup>-</sup> )	Diels-Alder polymerization (3.1)	4, 20
	TMAC6PP	1.74				126 (- <sup>c</sup> , OH <sup>-</sup> )	17 (rt, Cl <sup>-</sup> )		20
Ni-catalyzed poly(phenylene)	QPAF-TMA	1.26	49	24 (80, 60)	218 (80, 60)	45 (30, OH <sup>-</sup> )	50 (30, OH <sup>-</sup> )	Ni-catalyzed coupling reactions (3.2)	44
	QPAF-DMBA	1.33	252			53 (30, OH <sup>-</sup> )	87 (30, OH <sup>-</sup> )		45
	QPAF-4	1.47	276	23 (80, 60)	270 (80, 60)	105 (30, OH <sup>-</sup> )	86 (80, OH <sup>-</sup> )		47
	PPMB	2.56	129 <sup>d</sup>	72 (21, 42)	49 (21, 42)	81 (22, OH <sup>-</sup> / HCO <sub>3</sub> <sup>-</sup> )	13 (22, OH <sup>-</sup> / HCO <sub>3</sub> <sup>-</sup> )		48
	BPN1-65	1.94	139	33 (50, 50)	100 (50, 50)	85 (80, OH <sup>-</sup> )	88 (80, OH <sup>-</sup> )		55
Acid-catalyzed polymer	BPN1-100	2.70	110	20 (50, 50)	40 (50, 50)	124 (80, OH <sup>-</sup> )	122 (80, OH <sup>-</sup> )	Acid-catalyzed Friedel-Crafts polyhydroxy alkylation (3.3)	55
	<i>m</i> -TPN1	2.18	126	29 (50, 50)	35 (50, 50)	70 (80, OH <sup>-</sup> )	112 (80, OH <sup>-</sup> )		56
	PTPipQ6	2.08				44 (20, OH <sup>-</sup> )	48 (20, OH <sup>-</sup> )		58
	QAPPT	2.65		35 (rt, - <sup>c</sup> )	40 (rt, - <sup>c</sup> )		137 (80, OH <sup>-</sup> )		59
Blended spiro-ionene	S70P30	4.0 <sup>c</sup>	80 ( $M_n$ ) <sup>e</sup>			220 (90, OH <sup>-</sup> )	120 (90, OH <sup>-</sup> )	Cyclo-polycondensation (3.4)	68
poly(dimethyl benzimidazolium)	Mes-PDMBI <sup>f</sup>	2.0				162 (25, OH <sup>-</sup> /HCO <sub>3</sub> <sup>-</sup> )	9.6 (25, OH <sup>-</sup> /HCO <sub>3</sub> <sup>-</sup> )	Others (3.5)	74
	HMT-PMBI	2.0				42 (22, OH <sup>-</sup> /HCO <sub>3</sub> <sup>-</sup> )	1.4 (22, OH <sup>-</sup> /HCO <sub>3</sub> <sup>-</sup> )		75
poly(arylene imidazolium)	HMT-PMPI	2.61	67	44 (- <sup>c</sup> )	44 (- <sup>c</sup> )	82 (25, OH <sup>-</sup> /HCO <sub>3</sub> <sup>-</sup> )	14 (25, OH <sup>-</sup> /HCO <sub>3</sub> <sup>-</sup> )		76
<b>Aryl ether-containing polyaromatics</b>									
Partially fluorinated poly(arylene ether)	QPE-bl-9	2.0	319	7 (80, 60)	5 (80, 60)	70 (30, OH <sup>-</sup> )	138 (80, OH <sup>-</sup> )		61
	6QA-4	2.23		6 (rt, - <sup>c</sup> )	7 (rt, - <sup>c</sup> )	59 (rt, - <sup>c</sup> )	21 (rt, OH <sup>-</sup> )		81
	PES-6-QA	1.48	73	9 (- <sup>c</sup> )	58 (- <sup>c</sup> )	78 (30, OH <sup>-</sup> )	63 (80, OH <sup>-</sup> )		23
Poly(ether sulfone)	AI-PES-6	1.20	471	52 (25, 50)	10 (25, 50)	12 (80, OH <sup>-</sup> )	110 (80, OH <sup>-</sup> )		82
	PDAPip4	2.02		21 (rt, - <sup>c</sup> )	22 (rt, - <sup>c</sup> )	45 (80, OH <sup>-</sup> )	102 (80, OH <sup>-</sup> )		83
Poly(arylene ether sulfone nitrile)	ImPESN-19-22	2.07	112	32 (rt, 60)	17 (rt, 60)	23 (60, - <sup>c</sup> )	15 (80, - <sup>c</sup> )		84

Poly(phenylene oxide)	50PPOFC6NC 6	1.89		16 (rt, - <sup>c</sup> )	22 (rt, - <sup>c</sup> )	97 (rt, OH <sup>-</sup> )	42 (rt, OH <sup>-</sup> )	85
<b>Polyolefins</b>								
Poly(ethylene)	AAEM-2	1.37	54 ( $M_n$ )	5 (- <sup>c</sup> )	140 (- <sup>c</sup> )	94 (rt, OH <sup>-</sup> )	59 (50, OH <sup>-</sup> )	86
Poly(styrene) block copolymer	C30D70-1.7	1.65	15 ( $M_n$ ) <sup>g</sup>	3 (80, 85)	180 (80, 85)	117 (22, OH <sup>-</sup> )	98 (22, OH <sup>-</sup> )	87
Poly(propylene)	PP-TMA-20	1.56	148	17 (rt, 30)	328 (rt, 30)	34 (20, OH <sup>-</sup> )	17 (20, OH <sup>-</sup> )	12
SEBS	SEBS-TMA	2.19	114	6 (50, 50)	330 (50, 50)	211 (rt, OH <sup>-</sup> )	102 (80, OH <sup>-</sup> )	88
Poly(4-methyl- 1-pentene)	PMP-TMA-41	1.92	113	3 (rt, 30)	111 (rt, 30)	29 (20, OH <sup>-</sup> )	43 (20, OH <sup>-</sup> )	89
Radiation- grafted ETFE	RG-AEM (E- 5)	2.13		25 (- <sup>c</sup> ) <sup>h</sup>	205 (- <sup>c</sup> ) <sup>h</sup>	57 (rt, OH <sup>-</sup> )	68 (80, Cl <sup>-</sup> )	90

<sup>a</sup>The values in brackets represent the temperature (°C) and the relative humidity (%) of the measurement condition. <sup>b</sup>The values in brackets represent the temperature (°C) and the counter anion of the measurement condition. <sup>c</sup>Not specified. <sup>d</sup>The value was calculated from intrinsic viscosity. <sup>e</sup>The values are from spiro-ionene **2** before blending. <sup>f</sup>25% poly(benzimidazole) and 75% Mes-PDMBI blend membrane. <sup>g</sup>The value is from PA-*b*-XS before cross-linking. <sup>h</sup>Mechanical strength for relative comparison, not absolute mechanical properties against ASTM standards.

#### 4.1 Mechanical Properties

A mechanically robust and tough AEM is required for high AMFC operational performance and long-term durability. A critical molecular weight must be reached to promote intermolecular chain entanglement, which is required for good mechanical strength and membrane flexibility. Further increase beyond the critical molecular weight keeps improving mechanical properties, but the degree of mechanical property improvement is less and polymer processibility is lowered. In the case of polyaromatics, relatively high molecular weight is required to form thin films ( $\leq 30 \mu\text{m}$ ); quaternized polyaromatics having linear polymer backbone structure, such as BPN1, typically require number-average molecular weight ( $M_n$ ) of  $> 50 \text{ kg/mol}$  to make flexible AEMs.<sup>55</sup> For those with more bulky and rigid backbone structure, for instance, DAPP-type polymers, often require  $> 80 \text{ kg/mol}$  of  $M_n$ .<sup>4</sup> The molecular weight of the polymers affects membrane mechanical properties; both tensile strength and elongation at break of ATMPP increased from 28 to 32 MPa and from 19 to 47%, respectively, upon the molecular weight increase from 77 to 196 kg/mol (Table 2).

Due to the rigid nature of the backbone, quaternized polyaromatic AEMs usually show higher tensile strength and lower ductility than polyolefinic AEMs. As summarized in Table 2, most quaternized aryl ether-free polyaromatics with reasonably high molecular weight show the

high tensile strength (20–72 MPa) and low elongation at break (28–49%), while typical polyolefin-based AEMs tend to show lower tensile strength (3–17 MPa) and higher elongation at break ( $\geq 111\%$ ) (poly(ethylene),<sup>86</sup> poly(propylene),<sup>12</sup> polystyrene-*b*-poly(ethylene-*co*-butylene)-*b*-polystyrene (SEBS)<sup>88</sup> and radiation-grafted poly(ethylene-*co*-tetrafluoroethylene) (ETFE)<sup>90</sup>). The mechanical properties of quaternized aryl ether-free polyaromatics were even better than those polyaromatics with heteroatoms and polar groups in the backbone (Table 2), due to the more rigid phenyl-based backbone structure and the absence of polymer backbone degradation during the hydroxide ion exchange process.

Incorporation of aliphatic units in the backbone helps to increase elongation at break of polyaromatics, as demonstrated in mechanical properties of PAFs.<sup>44, 46, 47</sup> The polymer backbone with the flexible perfluorinated aliphatic portion exhibited much-enhanced elongation properties ( $> 200\%$ ); however, the gain in elongation properties is often at the cost of a loss of tensile strength ( $< 24$  MPa). When the perfluoroalkylene portion in the backbone decreased, the tensile strength increased but the elongation at break decreased.<sup>44</sup> This trade-off needs to be accounted for molecular design for polymer electrolytes to obtain the optimum mechanical properties of the materials.

#### 4.2 Water Uptake and Hydroxide Conductivity

Water uptake of ion exchange polymers is of fundamental significance because it is closely related with ion conductivity, mechanical properties, and gas permeability. The increase in ion contents in a membrane increases water uptake, which will facilitate ion mobility and enhance conductivity. For AEM applications, a certain level of IEC is required ( $> 1.5$  meq./g) to achieve a reasonable level of hydroxide ion conductivity for AEM applications (QPAF-DMBA with 0.63 meq./g IEC showed  $< 10$  mS/cm hydroxide conductivity at 30 °C<sup>45</sup>). When water uptake is beyond a certain level, the absorbed water will dilute the conductive species, resulting in lower conductivity

(PTPipQ1 with 145 wt.% water uptake showed lower hydroxide conductivity than PTPipQ6 with 44 wt.% water uptake<sup>58</sup>). Moreover, too much water uptake will lead to excessive swelling, which sacrifices the mechanical and dimensional stability of the membranes. Therefore, it is necessary to design a membrane material that can achieve high hydroxide ion conductivity while maintaining a reasonable level of water uptake.

For ionomer applications, quarternized polyaromatics with higher IECs than AEM materials are more favorable with Pt-based catalysts, which is counterintuitive. For acidic PEMFC system, typically polyaromatic ionomers with slightly lower IECs than AEM materials exhibited better performance because the cathode electrode bonded with ionomers having > 60 wt.% water uptake is prone to flood.<sup>91</sup> For AMFC system, the H<sub>2</sub> electrode flooding is not significant as much as in the O<sub>2</sub> electrode in PEMFC, although H<sub>2</sub> mass transport issue is still one of the biggest issues for the AMFCs. In addition, attaching more cationic functional groups help to desorb undesirable phenyl group adsorption on catalysts.<sup>92</sup> When less hydrophobic catalysts such as palladium, nickel at the anode or N-doped carbon at the cathode, it is necessary to use ionomers having lower water uptake to prevent the electrode flooding.

Fig. 9 demonstrates the hydroxide conductivity as a function of the water uptake of different backbone quaternized polymers. In a close IEC range around room temperature, quaternized polyaromatics with rigid backbones, with or without C–O bonds, tend to show lower water uptake compared to polyolefinic AEMs, which indicates having polyaromatic backbone helps to sustain a relatively lower level of water uptake. The PAF polymers with an aliphatic portion in the backbone tend to show higher water uptake, behaving more like polyolefinic AEMs.<sup>46, 47</sup> Having some cation structures with lower hydration energy, such as piperidinium, helped the membranes to have lower water uptake.<sup>60</sup> Regardless of lower water uptake, hydroxide conductivity of

quaternized aryl ether-free polyaromatics was competitive compared to other types of AEMs. However, spiro-ionenes and poly(dimethyl benzimidazolium)-type of polymer electrolytes, which contain ionic groups as part of their backbone, tend to show high water uptake and low ion conductivity (Table 2: S70P30, Mes-PDMBI, HMT-PMBI and HMT-PMPI) because the cations on the backbone provide more water absorption and have limited mobility for effective anion transport.

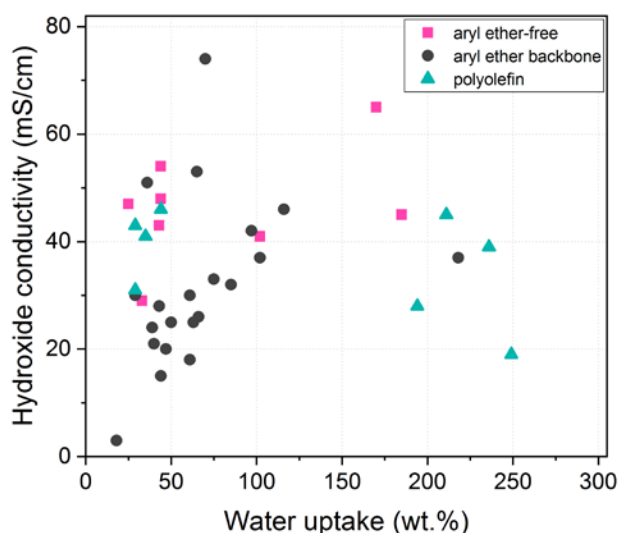


**Fig. 9** Water uptake ( $\text{OH}^-$ ) and hydroxide conductivity of AEMs with 1.8–2.2 meq./g IEC under room temperature, published since Jan. 2014. See Table S1 for the numerical values.

Most quaternized polymers show approximately twice higher hydroxide conductivity at  $\sim 80^\circ\text{C}$  compared to that at room temperature, exhibiting similar Arrhenius-type temperature dependence of the ion conductivity, regardless of the backbone structure (*m*-TPN1: 54 ( $30^\circ\text{C}$ ), 112 ( $80^\circ\text{C}$ ) mS/cm; S70P30: 49 ( $20^\circ\text{C}$ ), 120 ( $90^\circ\text{C}$ ) mS/cm; PDApip4: 51 (rt), 120 ( $90^\circ\text{C}$ ) mS/cm; SEBS-TMA: 45 ( $30^\circ\text{C}$ ), 102 ( $80^\circ\text{C}$ ) mS/cm).<sup>56, 68, 83, 88</sup>

### 4.3 Alkaline stability

Alkaline stability of polymer electrolytes, including backbone and ion-conductive cationic groups, is a critical requirement for practical applications of the AMFCs. Generally, the film form of the

polymer electrolytes is immersed in the aqueous alkaline solution in elevated temperature, and after a certain period the *ex situ* stability is measured by IEC change, conductivity change, and/or by NMR analysis for any structural difference, if it is still remaining soluble.<sup>93</sup> In the case of highly soluble polymer electrolytes, they are often dissolved in an NMR solvent and their spectrum is recorded during/after the measurement.<sup>68, 74-76</sup> The alkaline stability measurement condition is subjective and varies from one study to the next (concentration: 1–10 M aqueous NaOH or KOH solution;<sup>76</sup> temperature: rt–100 °C;<sup>60, 76</sup> time: 168–2200 h<sup>60</sup>), which makes the direct comparison of different polymer electrolytes difficult.

Table 3 summarizes the alkaline stability of the recently reported AEMs categorized by the polymer backbone structure. Since the polymer backbone of aryl ether-free polyaromatics is chemically stable, the alkaline stability of cation group and the linkage between the cation group and polymer backbone plays a significant role; TMAC6PP and QPAF-4 with cations tethered by a long alkyl spacer showed higher stability than ATMPP<sup>20</sup> and QPAF-TMA<sup>47</sup> with BTMA groups. While the presence of alkyl extender chains in alkyl QA cations increases the alkaline stability (QPAF-DMBA with a butyl extender chain showed higher stability than QPAF-TMA<sup>45</sup>), the alkyl extender chains from the piperidinium cation center destabilize the piperidinium ring and cause faster degradation by ring-opening elimination (PTPipQ8 with an octyl extender chain showed much faster degradation than dimethylpiperidinium-functionalized PTPipQ1<sup>58</sup>). Although dimethylpiperidinium cations are known for the high alkaline stability due to the constrained geometry of the rings, highly unfavorable towards hydroxide-initiated degradation,<sup>15</sup> there is some evidence of chemical degradation when they become part of polymer backbone chain, as shown in 10 M alkaline stability test of QAPPT.<sup>59</sup>

**Table 3** Alkaline stability of different backbone AEMs.

Polymer backbone	Cationic group	Sample name	Test condition		Duration (h)	% $\sigma$ or IEC loss	ref
			Conc. (M)	Temp. ( $^{\circ}$ C)			
<b>Aryl ether-free polyaromatics</b>							
DAPP	BTMA	ATMPP	4	80	1800	30 ( $\sigma$ )	94
	TMHA	TMAC6PP	4	80	2200	<5 (IEC)	
Poly(fluorene)	TMHA	PFBFF	1	80	720	<5 (IEC)	41
	BTMA	QPAF-TMA	1	80	1000	95 ( $\sigma$ )	
Ni-catalyzed poly(phenylene)	DMBA	QPAF-DMBA	1	80	500	<5 ( $\sigma$ )	45
	TMHA	QPAF-4	1	80	1000	<5 ( $\sigma$ )	47
	Imidazolium	PPMB	2	80	168	5 (IEC)	48
	TMHA	BPN1-100	1	95	1440	8 (IEC)	95
Acid-catalyzed poly(phenylene)	TMHA	<i>m</i> -TPN1	1	95	1440	<5 (IEC)	
	Piperidinium	PTPipQ1	2	90	700	5 (IEC)	58
	Piperidinium	PTPipQ8	2	90	700	70 (IEC)	
	Piperidinium	QAPPT	1	80	210	5 (IEC)	59
			10	80	240	33 (IEC)	
Spiro-ionene	<i>N</i> -spirocyclic QA	Spiro-ionene 2	1	80	1896	<5 (IEC)	68
Poly(arylene imidazolium)	Imidazolium	HMT-PMPI	10	100	168	<5 (IEC)	76
<b>Aryl ether-containing polyaromatics</b>							
Partially fluorinated poly(arylene ether)	BTMA	QPE-bl-9	1	80	500	97 ( $\sigma$ )	61
Poly(arylene ether ketone)	BTMA	QPAEK-x	4	rt	168	17 ( $\sigma$ )	96
Poly(arylene ether sulfone ketone)	BTMA	QPE-bl-11	1	60	1000	66 (IEC)	97
Poly(ether sulfone)	BTMA	B-110-PSU-NMe <sub>3</sub> -OH	1	50	6	39 (IEC)	64
	TMHA	PES-6-QA	1	60	720	12 ( $\sigma$ )	23
Poly(fluorene sulfone)	Imidazolium	AEM	1	60	400	6 ( $\sigma$ )	98
Poly(arylene ether sulfone nitrile)	Imidazolium	ImPESN-19-22	2	60	600	67 ( $\sigma$ )	84
	Multication	T20NC6NC5N	1	80	500	10 ( $\sigma$ )	99
Poly(phenylene oxide)	TMHA	50PPOC6NC6	1	80	1000	7 ( $\sigma$ )	85
	Piperidinium	PPO-7bisQPi-1.7	1	90	192	9 ( $\sigma$ )	100
<b>Polyolefins</b>							
Poly(ethylene)	Imidazolium	AAEM-2	1	80	720	<5 ( $\sigma$ )	86
Poly(propylene)	BTMA	PP-TMA-20	5	80	700	14 ( $\sigma$ )	12
polystyrene- <i>b</i> -poly(ethylene- <i>co</i> -butylene)- <i>b</i> -polystyrene	BTMA	SEBS-TMA	1	80	672	8 ( $\sigma$ )	
	TMHA	SEBS-TMHA	1	80	672	22 ( $\sigma$ )	88
Poly(4-methyl-1-pentene)	Trimethylnonyl QA	PMP-TMA-41	10	80	700	7 ( $\sigma$ )	89
Radiation-grafted ETFE	Methylbenzyl pyrrolidinium	C1-AEM	1	80	672	27 (IEC)	
	Methylbutyl pyrrolidinium	C4-AEM	1	80	672	13 (IEC)	101

Most aryl ether-containing polyaromatics were subjected to the stability test in lower temperature (< 80  $^{\circ}$ C) and showed higher degrees of reduction in their IEC value and ion

conductivity, typically within 1000 hours (Table 3). The state-of-the-art polyolefinic AEMs also demonstrated some noticeable decrease in their properties after the treatment in high-temperature alkaline condition. In many cases, the alkaline stability of polyolefinic AEMs is determined by cationic group incorporated in the polymer backbone. Since the functionalization of alkaline stable functional groups such as alkyl side chain ammonium groups to the polyolefinic backbone is limited, the alkaline stability of polyolefinic AEMs is reported to be inferior to aryl ether-free polyaromatic AEMs. Moreover, polymer backbone degradation of polyolefinic AEMs was observed after 7 days of dilute NaOH treatment at 80 °C.<sup>102</sup> The comparison showed the remarkable thermochemical alkaline stability of quaternized aryl ether-free polyaromatics, which makes them promising candidates particularly for high-performing AMFCs.

## **5. Performance of Aryl Ether-Free Polyaromatics Measured in MEA**

The performance of AMFCs is largely dependent on not only the AEM and ionomer but also the electrocatalyst, electrode morphology, gas diffusion layer and operating conditions. Therefore, it is inadequate to assess AEM and ionomer performance by the performance of AMFCs. Therefore, in this section, we discuss the AEM and ionomer performance in MEA configuration without assessing their properties by overall AMFC performance.

### **5.1 AEM performance**

The performance of AEMs is assessed by the high-frequency resistance (HFR) of the MEA. HFR of a single cell is composed of the electronic resistance, membrane-electrode interfacial resistance, and ASR of the AEM.<sup>104</sup> Because the interfacial resistance is proportional to the dimensional change of the AEM from dry to wet conditions,<sup>105</sup> low water uptake of AEMs is a prerequisite for high-performing MEAs. Typically, polyaromatic AEMs with water uptake of less than 100% at 30 °C exhibit small interfacial resistance ( $\leq 0.01 \Omega \text{ cm}^2$ ). Well-designed aryl ether-free

polyaromatics with an IEC of 2.0 meq./g or higher exhibit less than 100 wt.% water uptake (see Section 4.2).

ASR of AEMs is determined by the hydroxide conductivity and the thickness of the AEMs. The hydroxide conductivity of most aryl ether-free polyaromatics with IEC of  $\sim 2.0$  meq./g ranged 60–120 mS/cm at 80 °C in water. Thin film forming capability of quaternized polyaromatics is largely determined by the molecular weights of the polymers. The ASR of state-of-the-art aryl ether-free polyaromatics is  $\sim 0.03 \Omega \text{ cm}^2$  at 80 °C,<sup>106</sup> which is the lowest level among AEMs.

Fig. 10 shows the change of the current density and ASR of an MEA employing a 40  $\mu\text{m}$ -thick TMAC6PP during 300 h AMFC life test at 80 °C.<sup>107</sup> The cell current density and ASR gradually decreased over time. However, after replenishing the cell with 0.5 M NaOH after 200 h of AMFC operation, the ASR of the AEM was completely recovered to the original value ( $0.05 \Omega \text{ cm}^2$ ) although the cell current density was partly recovered. This suggests that the ASR increase during the life test may be due to the carbonation or instability of Pt/C catalyst or cathode ionomer degradation,<sup>108</sup> yet not related to the AEM chemical degradation<sup>109</sup>. FT-IR analysis of the AEM before and after the life test showed no spectral change, confirming that the chemical structure of the TMAC6PP AEM remained stable after the life test. Maurya et al. measured the HFR of an MEA employing a 35  $\mu\text{m}$ -thick *m*-TPN1 at a constant current of  $0.3 \text{ A cm}^{-2}$ .<sup>110</sup> The initial cell HFR after the cell break-in ( $0.068 \Omega \text{ cm}^2$ ) was not changed after 350 h operation of AMFC at 80 °C. Another MEAs with piperidinium functionalized poly(phenylene)s also exhibit stable performance over the extended time at 80–95 °C, supporting that aryl ether-free aromatic AEMs are stable under AMFC operating conditions.<sup>59, 60</sup> Typically, aryl ether-free polyaromatics having good *ex situ* alkaline stability, *ca.* < 5% IEC or conductivity loss after 500 h, 1 M NaOH treatment

exhibited no trace of membrane degradation when the membranes were used in MEAs for a couple hundred hours of AMFC operation.<sup>107</sup>

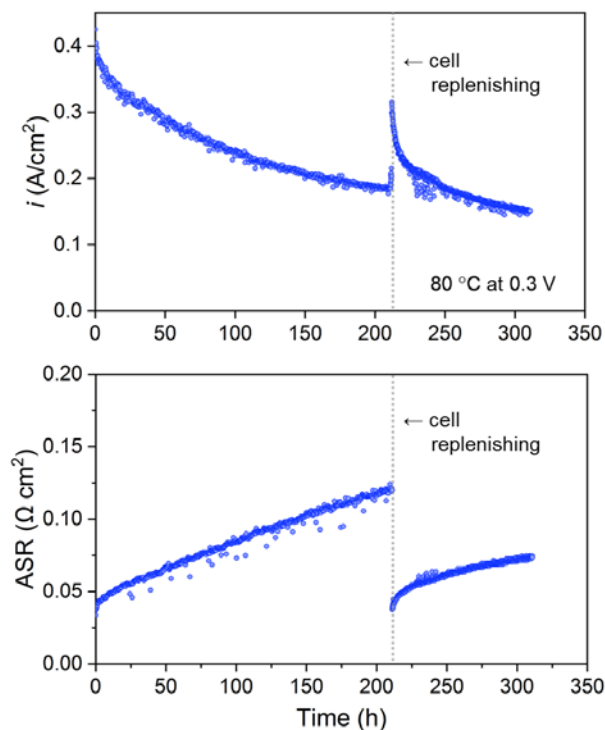


**Fig. 10** Long-term AMFC test of an MEA employing a 40  $\mu\text{m}$ -thick TMAC6PP at the constant voltage of 0.3 V. The life test was performed under  $\text{H}_2/\text{O}_2$ , 147 kPa backpressure. AEM: 40  $\mu\text{m}$ -thick TMAC6PP; ionomer: TMAC6PP; catalyst: commercial Pt/C ( $0.2 \text{ mg}_{\text{Pt}}/\text{cm}^2$ ) for both anode and cathode; the cell was replenished after 211 hour of life test. Replenishing process: immerse MEAs in 0.5 M NaOH for 30 min followed by rinsed several times with warm water ( $60 \text{ }^\circ\text{C}$ ). No residual NaOH remained in the MEA, confirmed by the pH of the effluent water. The cell was reassembled and continued to the life test.

## 5.2 Ionomer performance

AMFC electrode performance may be influenced by the dispersionability of the ionomers. Ionomers in liquid media generally form colloidal particles rather than fully solubilized polymer chains.<sup>111, 112</sup> While polyolefinic electrolytes are typically non-dispersionable in any liquid media, most polyaromatic electrolytes with high IEC ( $> 1.5 \text{ meq./g}$ ) can be prepared as liquid dispersion using aprotic polar or alcoholic solvents. Since quaternized polyaromatics with the hydroxide

counterion have a stronger hydrogen bonding interactions (physical cross-linking) and thus lower dispersionability, most liquid dispersions of quaternized polyaromatic ionomers for the AMFC electrodes are prepared first with the polymer having halogen counterions ( $\text{Cl}^-$ ,  $\text{Br}^-$ , etc.), then converted to the hydroxide form after electrode processing. Complete removing of the adsorbed halogen ion species from the electrocatalyst surface is critical because strongly adsorbed halogen anions on catalyst surface may negatively influence on the AMFC performance and durability. Dispersing agents are another factor that may impact the electrode performance.<sup>91</sup> Generally, aprotic dispersing agents such as DMSO and dimethylacetamide (DMAc) have good dispersionability for quaternized polyaromatics. Alcoholic dispersing agents having the methyl to hydroxyl group ratio of 1:1, e.g. methanol and ethylene glycol, are the best dispersing agents among alcohols.<sup>113</sup> Alcoholic dispersing agents or their mixture with water create more porosity in the electrode, therefore, it can be used where reactant gas transport is limited.

One of the most significant factors that affect the AMFC performance of the MEAs employing aryl ether-free polyaromatic ionomers is the phenyl group adsorption on hydrogen oxidation reaction (HOR) catalyst surface. Even though most alkaline ionomers available today have phenyl groups in the polymer backbone and/or side chain, it was shown that the side chain cationic group substituted phenyl groups may have a less negative impact than non-cationic group substituted phenyl groups due to the competitive adsorption between cationic and phenyl groups.<sup>114</sup> Fig. 11 compares the impact of phenyl group adsorption on AMFC performance of MEAs with three aryl ether-free polyaromatics. The figure shows that AMFC performance of MEAs employing poly(phenylene) ionomer improves when less phenyl group adsorbing Pt-Ru catalyst at the anode was used instead of using Pt catalyst. The performance of Pt-Ru anode catalyzed AMFC increases with less phenyl group-containing anode binder, i.e. quaternized

poly(alkyl phenylene). The further performance improvement was achieved with poly(flourene) anode ionomer, which has non-phenyl group adsorbing characteristics due to the non-rotating bulky fluorene structure. The strategy to make polyaromatics attaching rotationally restricted polymer backbone seems to work well as another rotationally restricted piperidinium functionalized terphenylene ionomer also showed good performance.<sup>59</sup> When these non-phenyl group-adsorbing quaternized polyaromatics are used as anode binders, the AMFC performance difference between Pt and Pt-Ru anode catalysts becomes comparable.

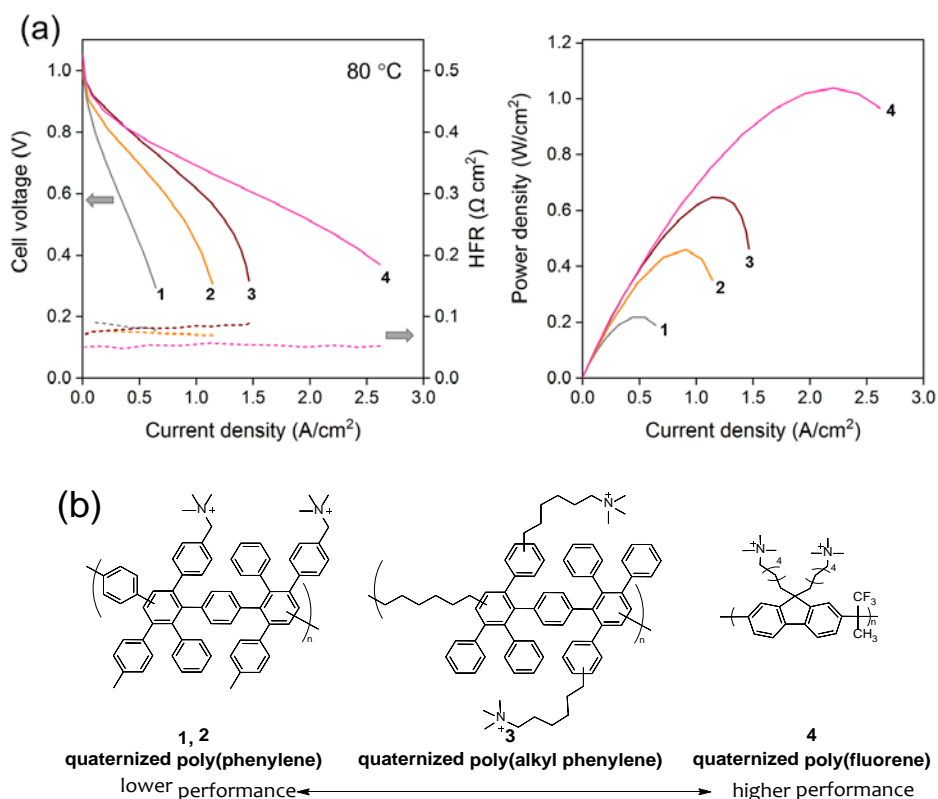


**Fig. 11** (a) Comparison of H<sub>2</sub>/O<sub>2</sub> AMFC performances of aryl ether-free polyaromatics using different anode composition and (b) ionomer structures used for the comparison: 1. quaternized poly(phenylene) (ATMPP) bonded Pt/C, 2. ATMPP-bonded Pt-Ru/C, 3. quaternized poly(alkyl phenylene) bonded Pt-Ru/C and 4. quaternized poly(flourene) bonded Pt-Ru/C. The AMFC performance was measured at 80 °C, 285 kPa backpressure under fully humidified conditions. Quaternized poly(phenylene) membranes (thickness= 30-50 μm) were used. Data was redrawn from Refs. 106 and 114.

### 5.3 AMFC performance

In this section, we compare the AMFC performance employing state-of-the-art polymer electrolytes with different backbone structure in order to illustrate the distinctiveness of aryl ether-free polymer electrolytes in MEAs. Fig. 12 shows the AMFC performance of MEAs with polyolefin, aryl ether-containing, and aryl ether-free polyaromatic polymer electrolytes.<sup>59, 102, 115-118</sup> The AMFCs employing polyolefin electrolytes exhibit the best performance among those, *ca.* the peak power density reached 1.5 and 2.0 W/cm<sup>2</sup> (Fig. 12a). There are several notes regarding to the good performance of polyolefin-based AMFCs: (i) the solid particulate dispersion of radiation-grafted ETFE ionomer was used to fabricate the electrodes of the MEAs, which was the only method due to the poor solubility of the ETFE ionomers, (ii) the performance was often measured at 60 °C rather than 80 °C probably because of the alkaline instability of the polyolefin electrolytes at 80 °C; the IEC loss of radiation grafted-LDPE and ETFE AEMs was negligible at 60 °C, *ca.* < 2 % after 1 M NaOH treatment for 7 days but notably increased at 80 °C, *ca.* 12% under the same condition,<sup>102</sup> (iii) the performance was measured without backpressure and sometimes under slightly lower humidification due to anode flooding, (iv) significant performance improvement was made with high reactant gas flow, *ca.* 1 L/min.

The AMFCs employing aryl ether-containing polyaromatic electrolytes exhibit relatively poor performance (Fig. 12b). The best AMFC performance employing an aryl ether-containing polyaromatic electrolyte was obtained with quaternized poly(aryl ether sulfone) (PES) by Zhuang et al. in 2015.<sup>117</sup> The peak power density of the PES cell reached 1.0 W/cm<sup>2</sup> when Pt-Ru/C catalyst was used at the anode. When Pt/C catalyst was used at the anode, the peak power density of the cell significantly reduced by 40%, *ca.* 0.6 W/cm<sup>2</sup>. Also, note that Zhuang et al. used a relatively high gas flow rate (0.4 L/min) for their 4 cm<sup>2</sup> cell. Later, Hickner et al. reported much lower cell

performance using a PPO electrolyte in 2017. The peak power density of the cell was 0.36 W/cm<sup>2</sup>. The low AMFC performance is partly attributed to the less-efficient Pt/C anode catalyst and low gas flow rate (0.25 L/min). More recent AMFC performance reported by other groups was even lower (the peak power density of ~0.2 W/cm<sup>2</sup>) with low gas flow rate (0.1 L/min).<sup>119-121</sup>

The AMFCs employing aryl ether-free polyaromatics exhibited better performance than that with aryl ether-containing polyaromatics. The best MEAs employing aryl ether-free polyaromatics was reported the peak power density of 1.5 W/cm<sup>2</sup> (Fig. 12c). One possible reason for better AMFC performance employing aryl ether-free polyaromatics can be the restrained rotation of phenyl groups in the ionomer backbone either by the fused five-member ring (polyfluorene) or the bulky piperidinium group attached to the main chain (QAPPT), which prevents phenyl group adsorption on the surface of HOR catalysts, as explained in Section 5.2. In other words, free rotation of phenyl groups via the aryl ether linkage in the aryl ether-containing polyaromatics can promote detrimental phenyl group adsorption. This is supported by the fact that less-phenyl group adsorbing Pt-Ru anode catalysts significantly improved the AMFC performance of the MEAs with aryl ether-containing polyaromatics yet only provided marginal impact to the AMFC performance employing aryl ether-free polyaromatics.<sup>59</sup>

The AMFC performance of MEAs employing aryl ether-free polyaromatics is lower than that of MEAs employing state-of-the-art polyolefin polymers. One potential reason for this is relatively thick AEM used for the polyaromatics cells; the thickness of polyaromatic AEMs used for AMFC performance evaluation is 30–50 μm, which is notably thicker than that of polyolefin AEMs (25 μm). Gottesfeld et al. indicated that a thinner AEM is beneficial to not only reducing cell resistance but also improving water management (preventing cathode dry out) and enhancing interfacial compatibility between AEM and electrodes.<sup>1</sup> Another possible reason is the absence of

phenyl ring in the polyolefin backbone. Although the aryl ether-free polyaromatic ionomers were designed to minimize the phenyl group adsorption, detrimental phenyl group adsorption may occur in a certain degree. There are two main differences in operating conditions between polyolefin- and aryl ether-free polyaromatic-based MEAs in order to achieve their best performance: (i) the performance of aryl ether-free polyaromatic-based AMFCs was typically measured at 80 °C and sometimes at 95 °C<sup>60</sup> to maximize catalyst efficiency as aryl ether-free polyaromatics are stable at the high operating temperatures, (ii) the performance of aryl ether-free polyaromatic-based AMFCs was measured with backpressure. This is because polyaromatic MEAs is less prone to flooding thus the performance keeps increasing with backpressure. The less severe flooding issue with AMFC MEAs employing polyaromatic ionomers is illustrated in Fig. S1 in which the performance of acidic and alkaline fuel cells employing aryl ether-free polyaromatics is compared. The performance of acidic PEMFC substantially decreased when humidification of water-generating cathode increased from 0 to 100%, indicating that the PEMFC cathode was flooded at 100% RH. In stark contrast, the performance of AMFC increased when humidification of water-generating anode increased from 0 to 100%, indicating that the AMFC anode was not flooded at 100% RH. Although AMFC anode flooding has been observed when polyaromatic ionomers having high water uptake or non-Pt electrode is used, this result shows that the anode flooding for quaternized aryl ether-free polyaromatic ionomer is a less significant issue with Pt-based catalysts. The reason for better water management of the electrodes with the radiation-grafted polyolefinic ionomer is unclear at this moment; it might be coming from high water uptake of the ionomer, non-uniform structure of the electrode driven by the particulate ionomer, or more water generated at the anode somehow helping to improve the performance of the polyolefinic ionomer.

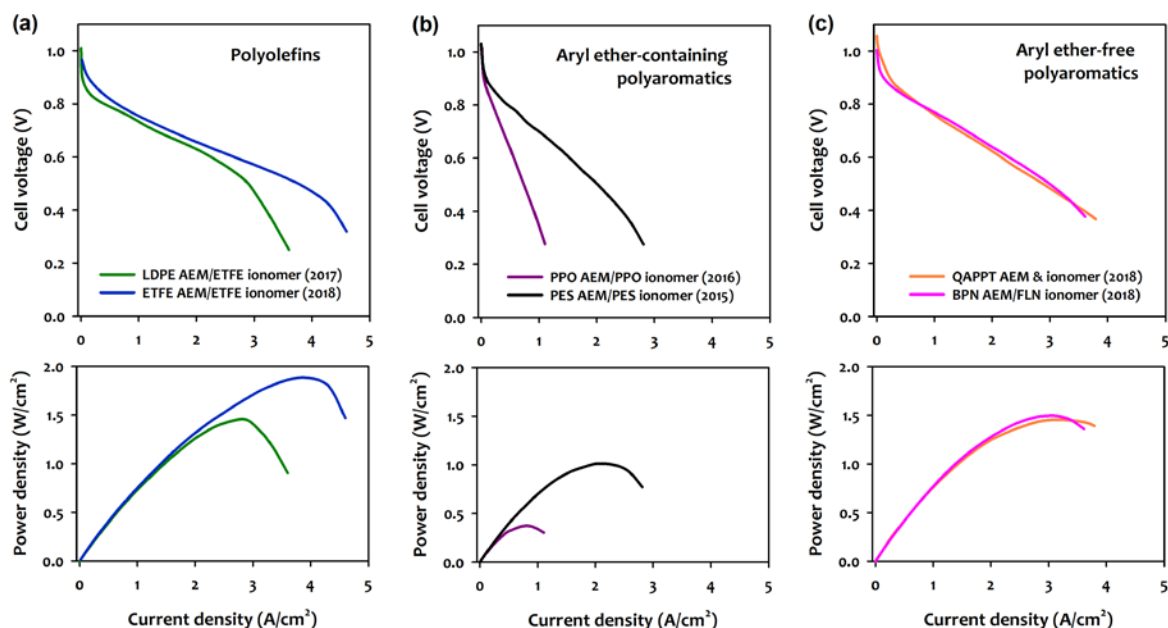


**Fig. 12** (a) Comparison of H<sub>2</sub>/O<sub>2</sub> AMFC performances employing (a) polyolefins, (b) aryl ether-containing polyaromatics and (c) aryl ether-free polyaromatics. **LDPE cell**: radiation-grafted LDPE AEM (25 μm dry thickness), radiation grafted particulate ETFE ionomer, Pt-Ru/C (50 wt.% Pt and 25 wt.% Ru) anode (0.4 mg<sub>Pt</sub> cm<sup>-2</sup>), Pt/C cathode (0.4 mg<sub>Pt</sub> cm<sup>-2</sup>); the performance was measured at 80 °C with 1.0 L/min flow for both electrodes (100% RH) without backpressure. **ETFE cell**: radiation-grafted ETFE AEM (25 μm dry thickness), radiation grafted particulate ETFE ionomer, Pt-Ru/C anode (50 wt.% Pt and 25 wt.% Ru) anode (0.4 mg<sub>Pt</sub> cm<sup>-2</sup>), Pt/C cathode (0.4 mg<sub>Pt</sub> cm<sup>-2</sup>); the performance was measured at 60 °C with 1.0 L/min flow for both electrodes (anode/cathode dew points = 45 °C/46 °C). **PPO cell**: PPO membrane (60 μm dry thickness) and ionomer, Pt/C anode and cathode (0.4 mg<sub>Pt</sub> cm<sup>-2</sup>); the performance was measured at 60 °C with 0.25 L/min flow for both electrodes with 0.1 MPa backpressure. **PES cell**: PES membrane (50 μm dry thickness) and ionomer, Pt-Ru/C anode (Ru atomic ratio: 0.2) anode (0.4 mg<sub>metal</sub> cm<sup>-2</sup>), Pt/C cathode (0.4 mg<sub>Pt</sub> cm<sup>-2</sup>); the performance was measured 0.4 L/min flow cathode and anode (100% RH) at 60 °C with 0.1 MPa backpressure. **QAPPT cell**: QAPPT membrane (30 μm dry thickness) and ionomer, Pt/C anode and cathode (0.4 mg<sub>Pt</sub> cm<sup>-2</sup>), cell performance was measured 0.12 L/min flow cathode and anode at 80 °C with 0.1 MPa backpressure. **BPN cell**: BPN membrane (35 μm thickness), FLN ionomer, Pt-Ru/C anode (0.5 mg<sub>Pt</sub> cm<sup>-2</sup> and 0.25 mg<sub>Ru</sub> cm<sup>-2</sup>), Pt/C cathode (0.6 mg<sub>Pt</sub> cm<sup>-2</sup>); the performance was measured at 80 °C with 2.0 L/min flow for anode and 1.0 L/min for cathode (100% RH) with 0.29 MPa backpressure. Data was redrawn from Refs. 59, 114-118.

It was also noted that high anode flow rate is beneficial to the performance of AMFC employing the aryl ether-free polyaromatics as well as polyolefin-based AMFCs. This suggests

that limited hydrogen gas access is still a performance-limiting factor. While low H<sub>2</sub> permeable polyaromatic ionomers may be one contributing factor to this issue as increasing the free volume of ionomer improves AMFC performance,<sup>122</sup> the limited hydrogen gas access may also be related with cation-hydroxide-water co-adsorption,<sup>123-126</sup> which occurs across the polymer electrolytes having methylammonium functional group. It has been observed that HOR on Pt is substantially inhibited by time-dependent and potential driven cation-hydroxide-water co-adsorption under alkaline conditions. Impedance analysis suggests that the inhibited HOR is largely due to the hydrogen permeability barrier through the accumulated co-adsorbed layer. In order to mitigate the co-adsorption, it might be useful to attach bulky cationic functional groups instead of methylammonium cations into the polymer structure as those bulky cationic groups have much less cation adsorption energy.<sup>127</sup>

## 6. Summary and Future Outlook

Quaternized aryl ether-free polyaromatics have a great potential for the use of AEMs and ionomers for AMFC applications because of their excellent chemical stability under high pH conditions. Currently, several synthetic processes are available to prepare quaternized aryl ether-free polyaromatics. Diels-Alder polymerization does not require metal catalysts and produces polymers made of wholly rigid phenyl backbone but lacks the ability to incorporate simply quaternizable moieties. Metal-catalyzed coupling reactions are able to produce various poly(phenylene) structures, and the choice of aryl monomers is critical since they may largely affect the properties of the resulting polymer electrolytes. Acid-catalyzed polyhydroxyalkylation produces polymers with QA precursors with high solubility in many polar solvents, but the choice of a monomer is important to grow high molecular weight polymers. Spiro-ionenes and poly(benzimidazolium)-types of polymer electrolytes synthesized by cyclo-polycondensation and others have high ion

contents in their backbone, which might require physical modification for the practical use. Because of the rigid aromatic groups in the polymer backbone, quaternized aryl ether-free AEMs require the high molecular weight to provide enough toughness as an AEM separator. Alternatively, the reinforcement embedded in the polyaromatic AEMs can provide necessary toughness for thin film AEMs. Good dispersionability of quaternized aryl ether-free polyaromatics in liquid media adds the value for the processing of ionomers. Diverse synthetic routes further enable to tailor their chemical structures to minimize undesirable interactions with electrocatalysts at the HOR potentials.

The AMFC performance of MEAs employing well-designed aryl ether-free polyaromatic electrolytes exhibits up to  $\sim 1.5 \text{ W cm}^{-2}$  under  $\text{H}_2/\text{O}_2$  conditions at  $80^\circ\text{C}$ . The AMFC performance reported with aryl ether-free polyaromatics is significantly better than that with aryl ether-containing polyaromatics but less than that with a state-of-the-art polyolefin. Implementing more robust and thinner AEMs may further improve the AMFC performance. The durability of the MEAs is yet demonstrated for a couple hundred hours, and further extended AMFC durability for thousands of hours needs to be demonstrated for practically viable applications, although the performance degradation occurs in the AMFC may also be associated with other AMFC components. Studies regarding ionomer degradation under low relative humidity AMFC environments<sup>108</sup> and possible oxidation due to the high potentials of AMFC cathode may need further to be investigated. Implementing low-PGM and non-PGM catalysts is also challenging. The aryl ether-free polyaromatic bonded low-PGM anode catalysts ( $\sim 0.025 \text{ mg}_{\text{Pt}} \text{ cm}^{-2}$ ) have been demonstrated,<sup>118</sup> but further lower loading with stable performance may be the next step. Implementing highly active non-PGM HOR and nitrogen-doped carbon-based non-PGM ORR catalysts is a tough nut to crack. In both cases, low reactant permeability through the electrodes

may be resolved. In addition, AEM and ionomer degradation with high peroxide generating non-PGM catalysts may further need to be investigated. Another technical barrier of AMFCs employing quaternized polyaromatic electrolytes is high cell resistance under low RH conditions. The performance of AMFC employing quaternized polyaromatic membranes shows high humidity dependence due to the increased cell resistance (Fig. S2), suggesting that the utilization of AEMs at high temperature ( $> 100\text{ }^{\circ}\text{C}$ ) with low humidity operating condition might be limited.

Focused programs with clear targets have been developed for AMFC devices and systems. A key component in meeting the goals is AEMs and ionomers. Further advancement of polymer electrolytes used as AEMs and ionomers will be useful not only for the provision of alkaline stable materials of high-performing AMFCs but also for the provision of the adaptation platform for other AEM-based electrochemical devices such as AEM water electrolysis,<sup>95</sup> high temperature PEMFCs,<sup>128, 129</sup> direct liquid fuel cells,<sup>130</sup> redox flow batteries,<sup>131</sup> and electrodialysis.<sup>132</sup> Quaternized aryl ether-free polyaromatics electrolytes exhibit desirable properties, including ion conductivity, mechanical toughness, thermal stability, processability, and lastly and most importantly, alkaline stability, which make them stand out as a promising candidate for the purpose.

## **Acknowledgments**

We thank Dr. Sandip Maurya for helpful discussion. This work was fully supported by the U.S. Department of Energy (US DOE), Office of Energy Efficiency and Renewable Energy (EERE), Fuel Cell Technologies Office (FCTO) under contract no. DE-AC52-06NA25396 (Los Alamos National Laboratory).

## References

1. S. Gottesfeld, D. R. Dekel, M. Page, C. Bae, Y. Yan, P. Zelenay and Y. S. Kim, *Journal of Power Sources*, 2018, **375**, 170-184.
2. G. Merle, M. Wessling and K. Nijmeijer, *Journal of Membrane Science*, 2011, **377**, 1-35.
3. P. Zschocke and D. Quellmalz, *Journal of membrane science*, 1985, **22**, 325-332.
4. C. Fujimoto, D.-S. Kim, M. Hibbs, D. Wroblewski and Y. S. Kim, *Journal of Membrane Science*, 2012, **423-424**, 438-449.
5. C. G. Arges and V. Ramani, *Proceedings of the National Academy of Sciences*, 2013, **110**, 2490-2495.
6. A. Amel, L. Zhu, M. Hickner and Y. Ein-Eli, *Journal of The Electrochemical Society*, 2014, **161**, F615-F621.
7. Y.-K. Choe, C. Fujimoto, K.-S. Lee, L. T. Dalton, K. Ayers, N. J. Henson and Y. S. Kim, *Chemistry of Materials*, 2014, **26**, 5675-5682.
8. A. D. Mohanty, S. E. Tignor, J. A. Krause, Y.-K. Choe and C. Bae, *Macromolecules*, 2016, **49**, 3361-3372.
9. S. Miyanishi and T. Yamaguchi, *Physical Chemistry Chemical Physics*, 2016, **18**, 12009-12023.
10. K. D. Kreuer, *Journal of Membrane Science*, 2001, **185**, 29-39.
11. K. J. T. Noonan, K. M. Hugar, H. A. Kostalik, E. B. Lobkovsky, H. D. Abruña and G. W. Coates, *Journal of the American Chemical Society*, 2012, **134**, 18161-18164.
12. M. Zhang, J. Liu, Y. Wang, L. An, M. D. Guiver and N. Li, *Journal of Materials Chemistry A*, 2015, **3**, 12284-12296.
13. J. S. Olsson, T. H. Pham and P. Jannasch, *Macromolecules*, 2017, **50**, 2784-2793.
14. A. D. Mohanty and C. Bae, *Journal of Materials Chemistry A*, 2014, **2**, 17314-17320.
15. M. Marino and K. Kreuer, *ChemSusChem*, 2015, **8**, 513-523.
16. A. D. Mohanty, S. E. Tignor, M. R. Sturgeon, H. Long, B. S. Pivovar and C. Bae, *Journal of The Electrochemical Society*, 2017, **164**, F1279-F1285.
17. B. R. Einsla, S. Chempath, L. Pratt, J. Boncella, J. Rau, C. Macomber and B. Pivovar, *ECS transactions*, 2007, **11**, 1173-1180.
18. S. Chempath, B. R. Einsla, L. R. Pratt, C. S. Macomber, J. M. Boncella, J. A. Rau and B. S. Pivovar, *The Journal of Physical Chemistry C*, 2008, **112**, 3179-3182.
19. N. Li, Y. Leng, M. A. Hickner and C.-Y. Wang, *Journal of the American Chemical Society*, 2013, **135**, 10124-10133.
20. M. R. Hibbs, *Journal of Polymer Science Part B: Polymer Physics*, 2013, **51**, 1736-1742.
21. H.-S. Dang and P. Jannasch, *Macromolecules*, 2015, **48**, 5742-5751.
22. P. Jannasch and E. A. Weiber, *Macromolecular Chemistry and Physics*, 2016, **217**, 1108-1118.
23. C. X. Lin, X. L. Huang, D. Guo, Q. G. Zhang, A. M. Zhu, M. L. Ye and Q. L. Liu, *Journal of Materials Chemistry A*, 2016, **4**, 13938-13948.
24. E. N. Hu, C. X. Lin, F. H. Liu, Q. Yang, L. Li, Q. G. Zhang, A. M. Zhu and Q. L. Liu, *ACS Applied Energy Materials*, 2018, DOI: 10.1021/acsaem.8b00698.
25. C. Ying, T. Yanping, W. Jinlei, Y. Shanzhong, C. Sheng, W. Haibing and D. Yunsheng, *Journal of Polymer Science Part A: Polymer Chemistry*, 2017, **55**, 1313-1321.
26. J. Wang, S. Gu, R. B. Kaspar, B. Zhang and Y. Yan, *ChemSusChem*, 2013, **6**, 2079-2082.
27. O. Diels and K. Alder, *European Journal of Organic Chemistry*, 1928, **460**, 98-122.

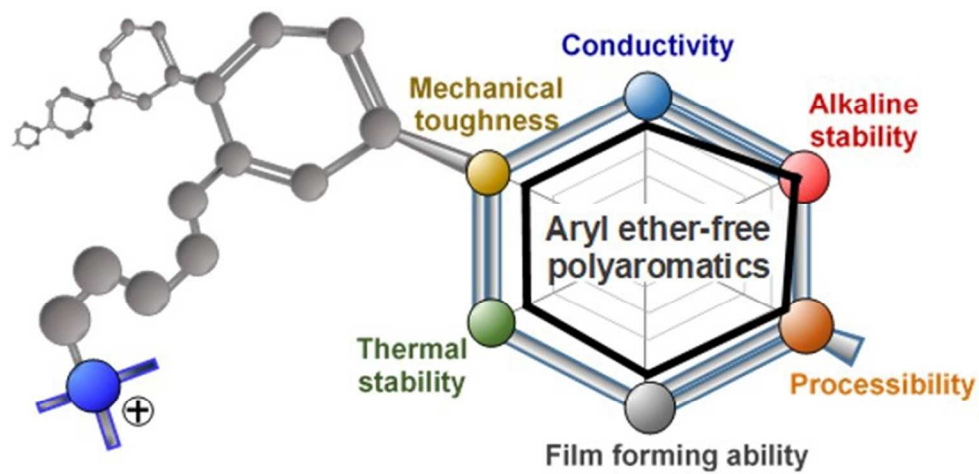
28. K. C. Nicolaou, S. A. Snyder, T. Montagnon and G. Vassilikogiannakis, *Angewandte Chemie International Edition*, 2002, **41**, 1668-1698.
29. J. Stille, F. Harris, R. Rakutis and H. Mukamal, *Journal of Polymer Science Part B: Polymer Letters*, 1966, **4**, 791-793.
30. C. H. Fujimoto, M. A. Hickner, C. J. Cornelius and D. A. Loy, *Macromolecules*, 2005, **38**, 5010-5016.
31. M. R. Hibbs, C. H. Fujimoto and C. J. Cornelius, *Macromolecules*, 2009, **42**, 8316-8321.
32. M. A. Ogliaruso and E. I. Becker, *The Journal of Organic Chemistry*, 1965, **30**, 3354-3360.
33. M. A. Ogliaruso, L. A. Shadoff and E. I. Becker, *The Journal of Organic Chemistry*, 1963, **28**, 2725-2728.
34. P. Kovacic and A. Kyriakis, *Journal of the American Chemical Society*, 1963, **85**, 454-458.
35. T. Largier, F. Huang and C. J. Cornelius, *European Polymer Journal*, 2017, **89**, 301-310.
36. Y.-J. Cheng, S.-H. Yang and C.-S. Hsu, *Chemical Reviews*, 2009, **109**, 5868-5923.
37. P. J. Stang, *Metal-catalyzed cross-coupling reactions*, John Wiley & Sons, 2008.
38. G. Kwiatkowski, M. Matzner and I. Colon, *Journal of Macromolecular Science, Part A: Pure and Applied Chemistry*, 1997, **34**, 1945-1975.
39. N. Miyaura and A. Suzuki, *Chemical Reviews*, 1995, **95**, 2457-2483.
40. A. Donat-Bouillud, I. Levesque, Y. Tao, M. D'Iorio, S. Beaupré, P. Blondin, M. Ranger, J. Bouchard and M. Leclerc, *Chemistry of materials*, 2000, **12**, 1931-1936.
41. W.-H. Lee, A. D. Mohanty and C. Bae, *ACS Macro Letters*, 2015, **4**, 453-457.
42. M. Ueda, Y. Miyaji, T. Ito, Y. Oba and T. Sone, *Macromolecules*, 1991, **24**, 2694-2697.
43. P. A. Havelka-Rivard, K. Nagai, B. D. Freeman and V. V. Sheares, *Macromolecules*, 1999, **32**, 6418-6424.
44. H. Ono, J. Miyake, S. Shimada, M. Uchida and K. Miyatake, *Journal of Materials Chemistry A*, 2015, **3**, 21779-21788.
45. A. M. A. Mahmoud, A. M. M. Elsaghier, K. Otsuji and K. Miyatake, *Macromolecules*, 2017, **50**, 4256-4266.
46. H. Ono, J. Miyake and K. Miyatake, *Journal of Polymer Science Part A: Polymer Chemistry*, 2017, **55**, 1442-1450.
47. H. Ono, T. Kimura, A. Takano, K. Asazawa, J. Miyake, J. Inukai and K. Miyatake, *Journal of Materials Chemistry A*, 2017, **5**, 24804-24812.
48. W. A. G., W. Thomas and H. Steven, *Angewandte Chemie International Edition*, 2016, **55**, 4818-4821.
49. H. Jang, S. Lee, J. Ha, K. Choi, T. Ryu, K. Kim, H.-S. Jeon and W. Kim, *Energies*, 2016, **9**, 271.
50. G. A. Olah, *Angewandte Chemie International Edition in English*, 1993, **32**, 767-788.
51. A. M. Diaz, M. G. Zolotukhin, S. Fomine, R. Salcedo, O. Manero, G. Cedillo, V. M. Velasco, M. T. Guzman, D. Fritsch and A. F. Khalizov, *Macromolecular Rapid Communications*, 2007, **28**, 183-187.
52. A. R. Cruz, M. C. G. Hernandez, M. T. Guzmán-Gutiérrez, M. G. Zolotukhin, S. Fomine, S. L. Morales, H. Kricheldorf, E. S. Wilks, J. Cárdenas and M. Salmón, *Macromolecules*, 2012, **45**, 6774-6780.

53. L. I. Olvera, M. T. Guzmán-Gutiérrez, M. G. Zolotukhin, S. Fomine, J. Cárdenas, F. A. Ruiz-Trevino, D. Villers, T. A. Ezquerro and E. Prokhorov, *Macromolecules*, 2013, **46**, 7245-7256.
54. O. Hernández-Cruz, M. G. Zolotukhin, S. Fomine, L. Alexandrova, C. Aguilar-Lugo, F. A. Ruiz-Treviño, G. Ramos-Ortíz, J. L. Maldonado and G. Cadenas-Pliego, *Macromolecules*, 2015, **48**, 1026-1037.
55. W.-H. Lee, Y. S. Kim and C. Bae, *ACS Macro Letters*, 2015, **4**, 814-818.
56. W.-H. Lee, E. J. Park, J. Han, D. W. Shin, Y. S. Kim and C. Bae, *ACS Macro Letters*, 2017, **6**, 566-570.
57. T. H. Marsilje, M. P. Hedrick, J. Desharnais, A. Tavassoli, Y. Zhang, I. A. Wilson, S. J. Benkovic and D. L. Boger, *Bioorganic & Medicinal Chemistry*, 2003, **11**, 4487-4501.
58. J. S. Olsson, T. H. Pham and P. Jannasch, *Advanced Functional Materials*, 2018, **28**, 1702758.
59. H. Peng, Q. Li, M. Hu, L. Xiao, J. Lu and L. Zhuang, *Journal of Power Sources*, 2018, **390**, 165-167.
60. J. Wang, Y. Zhao, B. P. Setzler, L. Wang, K. Hu, S. Rojas-Carbonell, B. Xu and Y. Yan, *Meeting Abstracts*, 2018, **MA2018-01**, 1751.
61. N. Yokota, M. Shimada, H. Ono, R. Akiyama, E. Nishino, K. Asazawa, J. Miyake, M. Watanabe and K. Miyatake, *Macromolecules*, 2014, **47**, 8238-8246.
62. J. Yan and M. A. Hickner, *Macromolecules*, 2010, **43**, 2349-2356.
63. H.-S. Dang, E. A. Weiber and P. Jannasch, *Journal of Materials Chemistry A*, 2015, **3**, 5280-5284.
64. A. D. Mohanty, Y.-B. Lee, L. Zhu, M. A. Hickner and C. Bae, *Macromolecules*, 2014, **47**, 1973-1980.
65. H. Noguchi and A. Rembaum, *Journal of Polymer Science Part B: Polymer Letters*, 1969, **7**, 383-394.
66. A. D. Wilson, *Developments in Ionic Polymers—2*, Springer Science & Business Media, 2012.
67. K. Müllen, J. Lex, R. C. Schulz and F. Walter, *Polymer Bulletin*, 1990, **24**, 263-269.
68. T. H. Pham, J. S. Olsson and P. Jannasch, *Journal of the American Chemical Society*, 2017, **139**, 2888-2891.
69. M. Ueda, M. Sato and A. Mochizuki, *Macromolecules*, 1985, **18**, 2723-2726.
70. J. A. Asensio, E. M. Sánchez and P. Gómez-Romero, *Chemical Society Reviews*, 2010, **39**, 3210-3239.
71. O. D. Thomas, K. J. Soo, T. J. Peckham, M. P. Kulkarni and S. Holdcroft, *Polymer Chemistry*, 2011, **2**, 1641-1643.
72. D. Henkensmeier, H. J. Kim, H. J. Lee, D. H. Lee, I. H. Oh, S. A. Hong, S. W. Nam and T. H. Lim, *Macromolecular Materials and Engineering*, 2011, **296**, 899-908.
73. B. Lin, H. Dong, Y. Li, Z. Si, F. Gu and F. Yan, *Chemistry of Materials*, 2013, **25**, 1858-1867.
74. O. D. Thomas, K. J. Soo, T. J. Peckham, M. P. Kulkarni and S. Holdcroft, *Journal of the American Chemical Society*, 2012, **134**, 10753-10756.
75. A. G. Wright and S. Holdcroft, *ACS Macro Letters*, 2014, **3**, 444-447.
76. J. Fan, A. G. Wright, B. Britton, T. Weissbach, T. J. Skalski, J. Ward, T. J. Peckham and S. Holdcroft, *ACS Macro Letters*, 2017, **6**, 1089-1093.

77. T. Yamaguchi, H. Zhou, S. Nakazawa and N. Hara, *Advanced Materials*, 2007, **19**, 592-596.
78. H. Jung, K. Fujii, T. Tamaki, H. Ohashi, T. Ito and T. Yamaguchi, *Journal of membrane science*, 2011, **373**, 107-111.
79. J.-H. Kim, E. J. Park, D.-K. Lim, B. Singh, C. Bae and S.-J. Song, *Journal of The Electrochemical Society*, 2015, **162**, F1159-F1164.
80. G. S. Sailaja, S. Miyanishi and T. Yamaguchi, *Polymer Chemistry*, 2015, **6**, 7964-7973.
81. Y. He, X. Ge, X. Liang, J. Zhang, M. A. Shehzad, Y. Zhu, Z. Yang, L. Wu and T. Xu, *Journal of Materials Chemistry A*, 2018, **6**, 5993-5998.
82. A. H. Rao, S. Nam and T.-H. Kim, *Journal of Materials Chemistry A*, 2015, **3**, 8571-8580.
83. D. J. Strasser, B. J. Graziano and D. M. Knauss, *Journal of Materials Chemistry A*, 2017, **5**, 9627-9640.
84. A. N. Lai, L. S. Wang, C. X. Lin, Y. Z. Zhuo, Q. G. Zhang, A. M. Zhu and Q. L. Liu, *ACS Applied Materials & Interfaces*, 2015, **7**, 8284-8292.
85. L. Zhu, J. Pan, C. M. Christensen, B. Lin and M. A. Hickner, *Macromolecules*, 2016, **49**, 3300-3309.
86. W. You, K. M. Hugar and G. W. Coates, *Macromolecules*, 2018, **51**, 3212-3218.
87. X. Ren, S. C. Price, A. C. Jackson, N. Pomerantz and F. L. Beyer, *ACS applied materials & interfaces*, 2014, **6**, 13330-13333.
88. A. D. Mohanty, C. Y. Ryu, Y. S. Kim and C. Bae, *Macromolecules*, 2015, **48**, 7085-7095.
89. M. Zhang, C. Shan, L. Liu, J. Liao, Q. Chen, M. Zhu, Y. Wang, L. An and N. Li, *ACS applied materials & interfaces*, 2016, **8**, 23321-23330.
90. L. Wang, E. Magliocca, E. L. Cunningham, W. E. Mustain, S. D. Poynton, R. Escudero-Cid, M. M. Nasef, J. Ponce-González, R. Bance-Souahli and R. C. Slade, *Green Chemistry*, 2017, **19**, 831-843.
91. D. S. Kim, C. Welch, R. Hjelm, Y. S. Kim and M. D. Guiver, in *Polymer Science: A Comprehensive Reference*, 2012, vol. 10, p. 691.
92. I. Matanovic, H. T. Chung and Y. S. Kim, *The journal of physical chemistry letters*, 2017, **8**, 4918-4924.
93. Y. S. Kim and K. S. Lee, *Polym Rev*, 2015, **55**, 330-370.
94. Y. S. Kim, *2017 Annual Merit Review and Peer Evaluation Meeting, June 5-9, 2017.*, 2017, Project ID: FC 146.
95. E. J. Park, C. B. Capuano, K. E. Ayers and C. Bae, *Journal of Power Sources*, 2018, **375**, 367-372.
96. Z. Zhang, K. Shen, L. Lin and J. Pang, *Journal of Membrane Science*, 2016, **497**, 318-327.
97. R. Akiyama, N. Yokota, E. Nishino, K. Asazawa and K. Miyatake, *Macromolecules*, 2016, **49**, 4480-4489.
98. B. Lin, L. Qiu, B. Qiu, Y. Peng and F. Yan, *Macromolecules*, 2011, **44**, 9642-9649.
99. L. Zhu, J. Pan, Y. Wang, J. Han, L. Zhuang and M. A. Hickner, *Macromolecules*, 2016, **49**, 815-824.
100. H.-S. Dang and P. Jannasch, *Journal of Materials Chemistry A*, 2016, **4**, 11924-11938.
101. J. Ponce-Gonzalez, I. Ouachan, J. R. Varcoe and D. K. Whelligan, *Journal of Materials Chemistry A*, 2018, **6**, 823-827.

102. L. Q. Wang, J. J. Brink, Y. Liu, A. M. Herring, J. Ponce-Gonzalez, D. K. Whelligan and J. R. Varcoe, *Energ Environ Sci*, 2017, **10**, 2154-2167.
103. A. M. Ahmed Mahmoud and K. Miyatake, *Journal of Materials Chemistry A*, 2018, DOI: 10.1039/C8TA04310H.
104. B. S. Pivovar and Y. S. Kim, *J Electrochem Soc*, 2007, **154**, B739-B744.
105. Y. S. Kim and B. S. Pivovar, *J Electrochem Soc*, 2010, **157**, B1616-B1623.
106. S. Maurya, S. Noh, I. Matanovic, E. J. Park, C. Narvaez Villarrubia, J. Han, C. Bae and Y. S. Kim, 2018, **Submitted**.
107. Y. S. Kim, *Advanced Materials for Fully Integrated MEAs in AEMFCs*, US DOE EERE, Washington DC, 2017.
108. D. R. Dekel, M. Amar, S. Willdorf, M. Kosa, S. Dhara and C. E. Diesendruck, *Chemistry of Materials*, 2017, **29**, 4425-4431.
109. A. Zadick, L. Dubau, N. Sergent, G. Berthome and M. Chatenet, *ACS Catalysis*, 2015, **5**, 4819-4824.
110. S. Maurya, J. H. Dumont, C. Narvaez Villarrubia, I. Matanovic, D. Li, Y. S. Kim, S. Noh, J. Han, C. Bae, H. A. Miller, C. Fujimoto and D. R. Dekel, *Acs Catal*, 2018, submitted.
111. C. Welch, A. Labouriau, R. Hjelm, B. Orlor, C. Johnston and Y. S. Kim, *Acs Macro Letters*, 2012, **1**, 1403-1407.
112. Y. S. Kim, C. F. Welch, R. P. Hjelm, N. H. Mack, A. Labouriau and E. B. Orlor, *Macromolecules*, 2015, **48**, 2161-2172.
113. Y. S. Kim, *US Patent Application*, 2016, No. 15/204,523.
114. S. Maurya, C. Fujimoto, M. R. Hibbs, C. Narvaez Villarrubia and Y. S. Kim, *Chem. Mater.*, 2018, **30**, 2188-2192.
115. T. J. Omasta, A. M. Park, J. M. Lamanna, Y. Zhang, X. Peng, L. Wang, D. L. Jacobson, J. R. Varcoe, D. S. Hussey, B. Pivovar and W. E. Mustain, *Energ Environ Sci*, 2018, **11**, 551-558.
116. J. Pan, L. Zhu, J. J. Han and M. A. Hickner, *Chem Mater*, 2015, **27**, 6689-6698.
117. Y. Wang, G. W. Wang, G. W. Li, B. Huang, J. Pan, Q. Liu, J. J. Han, L. Xiao, J. T. Lu and L. Zhuang, *Energ Environ Sci*, 2015, **8**, 177-181.
118. Y. S. Kim, *2018 Annual Merit Review and Peer Evaluation Meeting, June 13-15, 2018.*, 2018, Project ID: FC 146.
119. Y. B. He, X. L. Ge, X. Liang, J. J. Zhang, M. A. Shehzad, Y. Zhu, Z. J. Yang, L. Wu and T. W. Xu, *J Mater Chem A*, 2018, **6**, 5993-5998.
120. C. X. Lin, H. Y. Wu, L. Li, X. Q. Wang, Q. G. Zhang, A. M. Zhu and Q. L. Liu, *Acs Appl Mater Inter*, 2018, **10**, 18327-18337.
121. Q. Yang, L. Li, C. X. Lin, X. L. Gao, C. H. Zhao, Q. G. Zhang, A. M. Zhu and Q. L. Liu, *J Membrane Sci*, 2018, **560**, 77-86.
122. E. J. Park, S. Maurya, C. Bae and Y. S. Kim, *Meeting Abstracts*, 2018, **MA2018-01**, 1753.
123. M. Unlu, D. Abbott, N. Ramaswamy, X. M. Ren, S. Mukerjee and P. A. Kohl, *J Electrochem Soc*, 2011, **158**, B1423-B1431.
124. H. T. Chung, U. Martinez, J. Chlistunoff, I. Matanovic and Y. S. Kim, *Journal of Physical Chemistry Letters*, 2016, **7**, 4464-4469.
125. X. T. Chen, I. T. McCrum, K. A. Schwarz, M. J. Janik and M. T. M. Koper, *Angew Chem Int Edit*, 2017, **56**, 15025-15029.

126. I. T. McCrum, M. A. Hickner and M. J. Janik, *Journal of The Electrochemical Society*, 2018, **165**, F114-F121.
127. H. Chung, Y. K. Choe, U. Martinez, I. Gonzalez, A. Mohanti, C. Bae and Y. S. Kim, *J Electrochem Soc*, 2016, **163**, F1503-F1509.
128. K. S. Lee, J. S. Spendelow, Y. K. Choe, C. Fujimoto and Y. S. Kim, *Nat Energy*, 2016, **1**.
129. K. S. Lee, S. Maurya, Y. S. Kim, C. R. Kreller, M. S. Wilson, D. Larsen, S. E. Elangovan and R. Mukundan, *Energ Environ Sci*, 2018, **11**, 979-987.
130. S. Alexey, P. Monica, R. A. J., A. Plamen, S. Tomokazu, A. Koichiro and T. Hirohisa, *Angewandte Chemie*, 2014, **126**, 10504-10507.
131. A. M. Pezeshki, Z. J. Tang, C. Fujimoto, C. N. Sun, M. M. Mench and T. A. Zawodzinski, *J Electrochem Soc*, 2016, **163**, A5154-A5162.
132. V. I. Zabolotskiy, A. Y. But, V. I. Vasil'eva, E. M. Akberova and S. S. Melnikov, *J Membrane Sci*, 2017, **526**, 60-72.



This review article presents a recent progress in the area of synthesis of quaternized aryl ether-free polyaromatics for alkaline membrane fuel cells.

118x81mm (150 x 150 DPI)